Received 12 March 2022; revised 8 April 2022; accepted 11 April 2022. Date of publication 13 April 2022; date of current version 25 April 2022.

*Digital Object Identifier 10.1109/OJCOMS.2022.3167101*

# User-Heterogeneous Cell-Free Massive MIMO Downlink and Uplink Beamforming via Tensor Decomposition

**KENGO ANDO [1] (Graduate Student Member, IEEE), HIROKI IIMORI [2] (Graduate Student Member, IEEE), GIUSEPPE THADEU FREITAS DE ABREU [2] (Senior Member, IEEE), AND KOJI ISHIBASHI [1] (Senior Member, IEEE)**

[1]Advanced Wireless and Communication Research Center, The University of Electro-Communications, Tokyo 182-8585, Japan

[2]Focus Area Mobility, Department of Electrical and Computer Engineering, Jacobs University Bremen, 28759 Bremen, Germany

CORRESPONDING AUTHOR: K. ANDO (e-mail: k.ando@awcc.uec.ac.jp)

This work was supported by JST SICORP, Japan, under Grant JPMJSC20C1.

**ABSTRACT** We consider a cell-free massive MIMO (CF-mMIMO) system in which multiple access points (APs), connected to a common central processing unit (CPU) through unbounded fronthaul, collaboratively serve multiple users in a heterogeneous scenario in which each user equipment (UE) has a different number of antennas, and therefore is capable of communicating via distinct numbers of digital streams. For such a user-heterogeneous system, new joint transmit (TX)/receive (RX) beamforming (BF) algorithms are then proposed, both for downlink and uplink modes and integrated with two alternative transmit (TX) power and spatial resource allocation strategies, which enable interference-free communications. To that end, a novel tensor decomposition scheme is presented, based on an orthogonality-enforcing modification of the recently-proposed multilinear generalized singular value decomposition (ML-GSVD). Simulation results show both that the new orthogonality-enforcing ML-GSVD (OEML-GSVD) achieves greater accuracy than the previous multilinear generalized singular value decomposition (ML-GSVD) without sacrificing convergence speed, and that the corresponding OEML-GSVD-based proposed beamformers outperform state-of-the-art (SotA) techniques, as well as an equivalent beamformer based on the previous ML-GSVD alternative.

**INDEX TERMS** Cell-free massive MIMO (CF-mMIMO), beamforming design, tensor factorization, multilinear generalized singular value decomposition (ML-GSVD).

## I. INTRODUCTION

THE INTERNET of Things (IoT) has been an early and strong force in the vision of fifth generation (5G) systems [1]. Recently, vehicle to everything (V2X) has taken an increasingly prominent role [2] in promoting the evolution of wireless systems beyond fifth generation (5G+). In fact, the stringent data-rate, coverage, reliability, and low-latency requirements of applications such as autonomous connected driving (ACD) are central motivations in various innovative technologies now under consideration for sixth generation (6G) systems [3].

A consolidated trend of 5G/6G systems is the expansion of services towards millimeter wave (mmWave) bands [4]–[6], which not only facilitates the employment of waveforms for simultaneous communications and sensing/localization [7], [8], both crucial to ACD applications, but also enables the incorporation of multiple-input multiple-output (MIMO) and massive MIMO (mMIMO) technologies. ndeed, meeting the demands of perceived zero latency and infinite capacity typical of applications such as ACD and augmented and virtual reality (AVR) would be almost impossible without the spectral and spatial resources brought by mmWave and mMIMO technologies [9]–[11].

After the initial excitement over the enormous potential of mMIMO demonstrated analytically [12], challenges of a practical nature were identified. In particular, with

regards to the scaling of the mMIMO approach [13]–[15], which quickly led to the emergence of the cell-free massive MIMO (CF-mMIMO) concept [16]–[18]. For example, it was shown in [19]–[21], that ideal optimized CF-mMIMO in fact has the potential to greatly improve the spectral efficiency of radio access in urban scenarios. A key to this is the careful design of joint transmit (TX) and receive (RX) beamforming (BF), conjugated with optimal resource allocation.

In light of the above, much recent work has sought to optimize various components of CF-mMIMO systems, including (to name but a few) pilot signaling [22]–[24], channel estimation [25], clustering [26], resource allocation [27], receiver design [28], and BF [29], [30]. However, a common factor among all the aforementioned contributions, and in the majority of the CF-mMIMO literature, is the assumption that user equipments (UEs) are equipped with the same number of antennas. This "homogeneity" assumption limits the practicality of corresponding methods, particularly in the context of beyond 5G and 6G systems for the IoT, which are quite to the contrary characterized by great heterogeneity among users, both in terms of the service requirements – which may for instance translate into distinct numbers of simultaneous digital streams per user – as well as in the specifications of corresponding devices, including different numbers of antennas at each UE.

In order to take full advantage of the spatial resources of CF-mMIMO systems, it is thus imperative to design optimization methods suited to heterogeneous setups in which UEs have arbitrary (*i.e.*, fundamentally distinct) numbers of antennas and digital streams [31], [32].

Focusing on BF design, the challenge posed by this user-heterogeneous paradigm can be readily understood when it is considered that the singular value decomposition (SVD) is well-known to be the key in the construction of optimal beamformers that maximize the spectral efficiency (SE) for MIMO communication systems under the assumption of perfect channel state information (CSI) and no interference [33]. With that in mind, a major problem is that extending the optimal SVD-based BF strategy requires the generalization of the SVD itself [34], which proves challenging outside special cases such as that of two users [35] and commutative matrices [36]. Motivated by similar problems, tensor algebra [37], [38] has recently emerged as a means to enable the joint decomposition of multiple matrices of different sizes (collected as slices of a tensor) in a manner such that some structure of the decomposed representations is shared [38].

Among these and other methods [39]–[41], a recently-introduced technique referred to as the multilinear generalized singular value decomposition (ML-GSVD) can be recognized as being particularly promising for application in multiuser MIMO problems [42]. In particular, the ML-GSVD scheme is a higher-order generalized singular value decomposition (HO-GSVD) which decomposes each of the complex-valued slices $\boldsymbol{H}_k$ of a tensor $\boldsymbol{\mathcal{H}}$ into the components $\boldsymbol{B}_k$, $\mathbf{C}_k$, and $\boldsymbol{A}^{\mathrm{T}}$, where $\boldsymbol{A}$ is common to all the slices. The details will be further discussed in Section III, but at this point it suffices to highlight that the interesting property of the ML-GSVD is that it exposes to the transmitter(s)/receiver(s) a common "interface" matrix (namely $\boldsymbol{A}^{\mathrm{T}}$), a feature that can then be exploited by the TX/RX beamformer(s) to separate streams to be sent to/by different users (in the downlink (DL)/uplink (UL), respectively).

However, a limitation of the ML-GSVD method in the context of TX/RX MIMO BF is that the technique in [42] is not designed to promote the separation of the subspaces of the common interface matrix $\boldsymbol{A}$, a feature that the method shares with other HO-GSVD approaches developed for applications in biochemistry (see e.g., [43]–[45]) and that does not facilitate the construction of TX beamformers.

This article is motivated by all the above, aiming at generalizing the well-known optimal SVD-based point-to-point MIMO BF scheme to a heterogeneous multi-user MIMO scenario, thus contributing to the area of CF-mMIMO system optimization as follows:

- *New Tensor Decomposition:* A variation of the recently-proposed ML-GSVD tensor decomposition method of [42] is presented, in which the orthogonalization of the subspaces in $\boldsymbol{A}$ is promoted by means of a procedure that enforces the sparsity in the matrix $\mathbf{C}$. As a result of this modification, the decomposition yields complete separation of all subspaces in $\boldsymbol{A}$, enabling interference-free BF designs in the underloaded case in which the number of spatial degrees $LN$ of $\boldsymbol{A}$ is larger than the total number of digital streams for the various users $\sum M_k$. In allusion to this feature, we refer to the novel technique here presented as the orthogonality-enforcing ML-GSVD (OEML-GSVD).
- *New BF Design via Tensor Decomposition:* Building on the aforementioned feature of the proposed OEML-GSVD, the design of joint TX/RX beamformers is presented both for the DL and the UL modes, which include two alternative power allocation schemes aiming at maximizing the system's total SE in either a greedy or a fairness-aware manner. Thanks to the sub-space separation induced by OEML-GSVD, the resulting tensor decomposition resembles the orthogonal sub-space separation of the conventional SVD. It is worth mentioning that the application of ML-GSVD is limited to the DL in the literature, indicating that this article is, to the best of our knowledge, the first attempt to apply such a tensor-based BF method also to UL communications.

In addition to the above, it is also confirmed via an extensive computer simulations and detailed complexity analysis that the proposed tensor-based BF outperform popular BF design alternatives with lower or similar complexity. We remark that as a consequence of the features of the OEML-GSVD, the overhead associated with centrally coordinated TX/RX beamforming is significantly reduced compared to existing schemes, since in the proposed method, only the

relatively small TX/RX BF matrices themselves need be distributed to UEs, as opposed to conventional methods which require the dissemination of much larger CSI matrices. It should be also be noted that although the OEML-GSVD and corresponding beamforming method is addressed here under the perfect CSI assumption, so as to enable direct comparison with preceding literature.

Finally, we recall that in the mMIMO literature, CF-mMIMO is regarded as a variation of mMIMO system – similar to virtual multiple-input multiple-output (MIMO), network MIMO, Distributed-MIMO (D-MIMO), and coordinated multipoint (CoMP) – in which antennas are distributed geographically and which operate in underloaded conditions [19]. In this article, we follow this common understanding and consider CF-mMIMO systems under the assumption that the spatial resources at the receiver is larger than the number of transmitter(s).

*Notation:* The following notation is used hereafter throughout the text. Real-valued column vectors and matrices are denoted by letters in bold face (e.g., $\mathbf{x}$) and capitalized bold face (e.g., $\mathbf{X}$), respectively, while their complex-valued counterparts are represented in corresponding italic boldface (e.g., $\boldsymbol{x}$ and $\boldsymbol{X}$), respectively. The $n$-th power of a matrix $\boldsymbol{X}$ is denoted as $\boldsymbol{X}^n$. Complex tensors are represented by bold capital letters in calligraphic font (*e.g.*, $\boldsymbol{\mathcal{X}}$), while $n$-th mode unfolding is denoted by $[\boldsymbol{\mathcal{X}}]_{(n)}$. The $\ell_1$, $\ell_2$ and Frobenius norms are denoted by $\|\cdot\|_1$, $\|\cdot\|_2$ and $\|\cdot\|_{\mathrm{F}}$, respectively. The transpose, conjugate, conjugate transpose, (pseudo-)inverse, capped pseudo-inverse, trace, vectorize, diagonalize and block diagonalize operations are represented as $(\cdot)^{\mathrm{T}}$, $(\cdot)^*$, $(\cdot)^{\mathrm{H}}$, $(\cdot)^{-1}$, $(\cdot)^{\dagger}$, $\mathrm{Tr}[\cdot]$, $\mathrm{vec}(\cdot)$, $\mathrm{diag}(\cdot)$, $\mathrm{blkdiag}(\cdot)$, respectively. The imaginary unit, the $N \times N$ identity matrix, the $N \times 1$ all-1 column vector, and the Khatri-Rao product are respectively denoted by $j$, $\mathbf{I}_N$, $\mathbf{1}_N$, and $\diamond$. The real and complex Gaussian distributions with mean $\nu_n$ and variance $\sigma_n^2$ are denoted by $\mathcal{N}(\nu_n, \sigma_n^2)$ and $\mathcal{CN}(\nu_n, \sigma_n^2)$, respectively.

## II. SYSTEM MODEL

Consider a CF-mMIMO system composed of $L$ access points (APs) distributed over a service area in a grid-like manner, each equipped with $N$ antennas and connected through wire fronthaul links to a single common central processing unit (CPU), and $K$ UEs, each equipped with a non-equal number $M_k$ of antennas, $k \in \mathcal{K}$, as illustrated in Fig. 1.

For the sake of simplicity, it is assumed that the wired fronthaul links from the APs to the CPU have an unlimited capacity (or considerably larger capacity compared with the data-traffic volume), and that multi-antenna UEs are uniformly and randomly located within a square with side length of $D$ [m]. In addition, we assume channel duality between UL and DL, and perfect CSI at both transmitter and receiver, in similarity to related literature such as [35], [42]. Following the original concept of CF-mMIMO systems [17], [19], [46], we consider the case in which the total spatial resources at the CPU is larger than that at the collection of UEs (*i.e.*, $LN > \sum_k M_k$), which is a common assumption in the literature on mMIMO and its variants. For the sake of generality, however, the proposed tensor decomposition algorithm to be introduced later is designed without this assumption, which is instead applied only in the simulations of Section IV, where the system model with specific antenna specifications is studied.

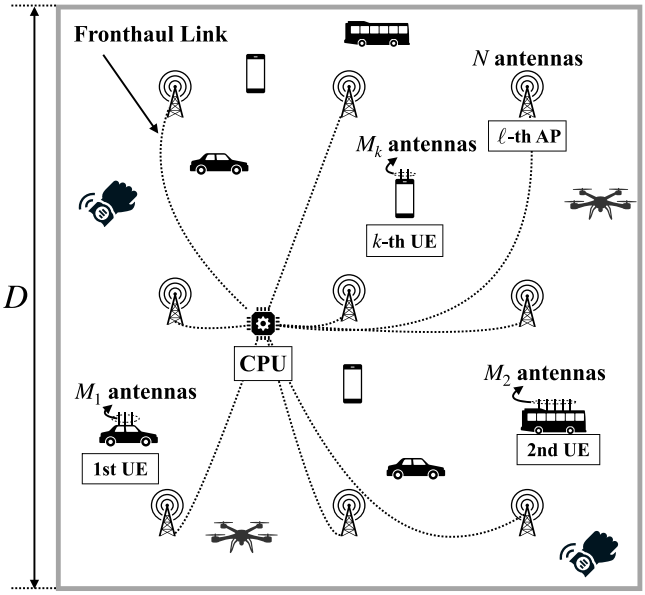


**FIGURE 1.** Illustration of a user-heterogeneous CF-mMIMO system.

Collecting the indices of all UEs and APs into the sets $\mathcal{K} \triangleq \{1, \ldots, K\}$ and $\mathcal{L} \triangleq \{1, \ldots, L\}$, respectively, and assuming that spatial correlation and fading affect the channel $\boldsymbol{H}_{\ell,k}$ between the $k$-th UE and the $\ell$-th AP, the latter can be modeled as [47], [48]

$$\boldsymbol{H}_{\ell,k} \triangleq \sqrt{10^{\frac{-\delta(d_{\ell,k})}{10}}} \boldsymbol{R}_{\ell,k}^{1/2} \boldsymbol{G}_{\ell,k} \left(\boldsymbol{T}_{\ell,k}^{1/2}\right)^{\mathrm{T}}, \ell \in \mathcal{L} \text{ and } k \in \mathcal{K}, \quad (1)$$

where $\boldsymbol{T}_{\ell,k} \in \mathbb{C}^{N \times N}$ and $\boldsymbol{R}_{\ell,k} \in \mathbb{C}^{M_k \times M_k}$ models the spatially correlated scattering at the $\ell$-th AP and $k$-th UE, respectively, the uncorrelated Gaussian matrix $\boldsymbol{G}_{\ell,k} \in \mathbb{C}^{M_k \times N}$ with $\mathrm{vec}(\boldsymbol{G}_{\ell,k}) \sim \mathcal{CN}(0, \mathbf{I}_{NM_k})$ captures the small-scale fading phenomena, while the mean channel power $\delta$ captures the large-scale fading coefficients determined by the urban macro cell path loss model given by $\delta(d_{\ell,k}) = 22.7 + 36.7 \log_{10}(d_{\ell,k}) + 26 \log_{10}(f_{\mathrm{c}})$ [49], where $f_{\mathrm{c}}$ denotes the carrier frequency and $d_{\ell,k}$ is the distance between the $\ell$-th AP and the $k$-th UE.

To further elaborate on equation (1), the spatial correlation matrices $\boldsymbol{T}_{\ell,k}$ and $\boldsymbol{R}_{\ell,k}$ result from the outer product of the array steering vectors at the $\ell$-th transmitting AP and the $k$-th receiving UE [48], respectively, which can be written as

$$\boldsymbol{T}_{\ell,k} \triangleq \boldsymbol{a}\left(\theta_{\ell,k}^t\right)\boldsymbol{a}\left(\theta_{\ell,k}^t\right)^{\mathrm{H}}, \quad (2a)$$

$$\boldsymbol{R}_{\ell,k} \triangleq \boldsymbol{a}\left(\theta_{\ell,k}^r\right)\boldsymbol{a}\left(\theta_{\ell,k}^r\right)^{\mathrm{H}}, \quad (2b)$$

where $\theta^t_{\ell,k}$ and $\theta^r_{\ell,k}$ denote the angles of departure (AoD) at the $\ell$-th AP and of arrival (AoA) at the $k$-th UE, respectively, and the array steering vector $\boldsymbol{a}(\cdot)$ corresponding to a uniform linear array (ULA) antenna with $N$ elements is given by

$$\boldsymbol{a}(\theta_{\ell,k}) \triangleq \left[1 e^{j\pi\cos\theta_{\ell,k}} \dots e^{j(N-1)\pi\cos\theta_{\ell,k}}\right]^{\mathrm{T}}. \tag{3}$$

Although we consider below two different scenarios (*i.e.*, uplink and downlink), the addressed scenario should not be confused with a full-duplex scenario (virtual or otherwise), in which uplink and downlink transmissions are simultaneous. The motivation of considering both uplink and downlink scenarios is to show that the proposed algorithm can be employed in both operation modes.

### A. DOWNLINK CASE

It will prove convenient to define the following effective DL channel matrix from the ensemble of APs to the $k$-th UE

$$\boldsymbol{H}_k \triangleq \left[\boldsymbol{H}_{1,k}, \boldsymbol{H}_{2,k}, \dots, \boldsymbol{H}_{L,k}\right] \in \mathbb{C}^{M_k \times LN}, \tag{4}$$

as well as the DL transmit and receive BF matrices $\boldsymbol{V}^{\mathrm{d}}_k \in \mathbb{C}^{LN\times Q_k}$ and $\boldsymbol{U}^{\mathrm{d}}_k \in \mathbb{C}^{Q_k\times M_k}$, respectively, such that the DL complex baseband signal $\boldsymbol{y}_k \in \mathbb{C}^{Q_k\times 1}$ at the $k$-th UE can be written as

$$\boldsymbol{y}_k = \overbrace{\boldsymbol{U}^{\mathrm{d}}_k\boldsymbol{H}_k\boldsymbol{V}^{\mathrm{d}}_k\boldsymbol{s}_k}^{\text{Intended signal at } k\text{-th UE}} + \overbrace{\sum_{k'=1,k'\neq k}^{K}\boldsymbol{U}^{\mathrm{d}}_k\boldsymbol{H}_k\boldsymbol{V}^{\mathrm{d}}_{k'}\boldsymbol{s}_{k'}}^{\text{Downlink inter-user interference}} + \overbrace{\boldsymbol{U}^{\mathrm{d}}_k\boldsymbol{n}_k}^{\text{Colored noise}}, \tag{5}$$

where $\boldsymbol{s}_k \in \mathbb{C}^{Q_k\times 1}$ denotes an informative symbol vector of length $Q_k$ while $\boldsymbol{n}_k \sim \mathcal{CN}(0,\sigma^2\mathbf{I}_{M_k})$ describes the additive white Gaussian noise (AWGN) vector at the $k$-th UE.

From equation (5), it follows that the DL spectral efficiency at the $k$-th UE is given by

$$\eta_k = \log_2\left(\det\left(\mathbf{I}_{M_k} + \boldsymbol{U}^{\mathrm{d}}_k\boldsymbol{H}_k\boldsymbol{F}^{\mathrm{TX}}_k\boldsymbol{H}^{\mathrm{H}}_k\boldsymbol{U}^{\mathrm{d}\mathrm{H}}_k\boldsymbol{E}^{\mathrm{d}^{-1}}_k\right)\right), \tag{6}$$

with $\boldsymbol{E}^{\mathrm{d}}_k \triangleq \sum_{k'=1,k'\neq k}^{K}\boldsymbol{U}^{\mathrm{d}}_k\boldsymbol{H}_k\boldsymbol{F}^{\mathrm{TX}}_{k'}\boldsymbol{H}^{\mathrm{H}}_k\boldsymbol{U}^{\mathrm{d}\mathrm{H}}_k + \sigma^2_k\boldsymbol{F}^{\mathrm{RX}}_k$, $\boldsymbol{F}^{\mathrm{TX}}_k \triangleq \boldsymbol{V}^{\mathrm{d}}_k\boldsymbol{V}^{\mathrm{d}\mathrm{H}}_k$ and $\boldsymbol{F}^{\mathrm{RX}}_k \triangleq \boldsymbol{U}^{\mathrm{d}}_k\boldsymbol{U}^{\mathrm{d}\mathrm{H}}_k$.

### B. UPLINK CASE

Similarly to the above, also for the UL we can define the following effective UL channel matrix from the $k$-th UE to the ensemble of APs

$$\boldsymbol{H}^{\mathrm{u}}_k \triangleq \left[\boldsymbol{H}_{1,k}, \boldsymbol{H}_{2,k}, \dots, \boldsymbol{H}_{L,k}\right]^{\mathrm{T}} = \boldsymbol{H}^{\mathrm{T}}_k \in \mathbb{C}^{LN\times M_k}, \tag{7}$$

where we highlight that the UL channel matrix is simply the transpose of its DL counterpart.

It follows from the definition of $\boldsymbol{H}^{\mathrm{u}}_k$ that the UL complex baseband signal $\boldsymbol{y} \in \mathbb{C}^{LN\times 1}$ received at the CPU as a result of transmissions from the UEs precoded by the UL transmit BF matrices $\boldsymbol{V}^{\mathrm{u}}_k \in \mathbb{C}^{M_k\times Q_k}$ can be written as

$$\boldsymbol{y} = \sum_{k=1}^{K}\boldsymbol{H}^{\mathrm{T}}_k\boldsymbol{V}^{\mathrm{u}}_k\boldsymbol{s}_k + \boldsymbol{n}, \tag{8}$$

where $\boldsymbol{s}_k \in \mathbb{C}^{Q_k\times 1}$ denotes the symbol vector of length $Q_k$ transmitted by the $k$-th UE and $\boldsymbol{n} \sim \mathcal{CN}(0,\sigma^2\mathbf{I}_{LN})$ describes the AWGN vector at the ensemble of APs.

The CPU then combines the UL signal described above via the BF matrices $\boldsymbol{U}^{\mathrm{u}}_k \in \mathbb{C}^{Q_k\times LN}$ in order to obtain the estimate of the $k$-th UE, yielding

$$\hat{\boldsymbol{s}}_k = \boldsymbol{U}^{\mathrm{u}}_k\boldsymbol{y} = \overbrace{\boldsymbol{U}^{\mathrm{u}}_k\boldsymbol{H}^{\mathrm{T}}_k\boldsymbol{V}^{\mathrm{u}}_k\boldsymbol{s}_k}^{\text{Intended } k\text{-th UE's signal}} + \overbrace{\sum_{k'=1,k'\neq k}^{K}\boldsymbol{U}^{\mathrm{u}}_k\boldsymbol{H}^{\mathrm{T}}_{k'}\boldsymbol{V}^{\mathrm{u}}_{k'}\boldsymbol{s}_{k'}}^{\text{Uplink inter-user interference}} + \overbrace{\boldsymbol{U}^{\mathrm{u}}_k\boldsymbol{n}}^{\text{Colored noise}}. \tag{9}$$

From equation (9), it follows that the UL spectral efficiency of the $k$-th UE is given by

$$\eta_k = \log_2\left(\det\left(\mathbf{I}_{Q_k} + \boldsymbol{U}^{\mathrm{u}}_k\boldsymbol{H}^{\mathrm{T}}_k\boldsymbol{G}^{\mathrm{TX}}_k\boldsymbol{H}^{*}_k\boldsymbol{U}^{\mathrm{u}\mathrm{H}}_k\boldsymbol{E}^{\mathrm{u}^{-1}}_k\right)\right), \tag{10}$$

with $\boldsymbol{E}^{\mathrm{u}}_k \triangleq \sum_{k'=1,k'\neq k}^{K}\boldsymbol{U}^{\mathrm{u}}_k\boldsymbol{H}^{\mathrm{T}}_{k'}\boldsymbol{G}^{\mathrm{TX}}_{k'}\boldsymbol{H}^{*}_{k'}\boldsymbol{U}^{\mathrm{u}\mathrm{H}}_k + \sigma^2\boldsymbol{G}^{\mathrm{RX}}_k$, $\boldsymbol{G}^{\mathrm{TX}}_k \triangleq \boldsymbol{V}^{\mathrm{u}}_k\boldsymbol{V}^{\mathrm{u}\mathrm{H}}_k$ and $\boldsymbol{G}^{\mathrm{RX}}_k \triangleq \boldsymbol{U}^{\mathrm{u}}_k\boldsymbol{U}^{\mathrm{u}\mathrm{H}}_k$.

We remark that for simplicity of notation in the above, we avoided using the superscripts $^{\mathrm{d}}$ and $^{\mathrm{u}}$ when not necessary. In particular, the quantities $\boldsymbol{y}_k$, $\boldsymbol{s}_k$, $\boldsymbol{s}_{k'}$ and $\boldsymbol{n}_k$ in equation (5), as well as $\eta_k$ in equation (6), all obviously refer to DL, while the quantities $\boldsymbol{y}$, $\boldsymbol{s}_k$, $\boldsymbol{n}$, $\hat{\boldsymbol{s}}_k$ and $\boldsymbol{s}_{k'}$ in equations (8) and (9), as well as $\eta_k$ in equation (10), all obviously refer to UL, such that the use of the superscripts on those quantities is unnecessary. In what follows, we shall also omit these superscripts when referring to the TX and RX beamformers whenever both cases can be considered interchangeably.

With that clarification, it is evident from equations (6) and (10) that the maximization of the system's DL and UL spectral efficiencies under the knowledge of the channel matrices $\boldsymbol{H}_k$ requires the joint optimization of the transmit and receive beamformers $\boldsymbol{V}_k$ and $\boldsymbol{U}_k$, respectively, for the corresponding DL and UL modes. And at this point, it will prove convenient to collect all $K$ components of each these key system matrices into system-wide quantities, which with $M_k \neq Q_k$ for different UEs, can be achieved via the introduction of tensor notation. In particular, define the tensors

$$\boldsymbol{\mathcal{H}} \triangleq \boxed{\boldsymbol{H}_1\boldsymbol{H}_K} = [\boldsymbol{H}_k]^K_1, \tag{11a}$$

$$\boldsymbol{\mathcal{V}} \triangleq \boxed{\boldsymbol{V}_1\boldsymbol{V}_K} = [\boldsymbol{V}_k]^K_1, \tag{11b}$$

$$\boldsymbol{\mathcal{U}} \triangleq \boxed{\boldsymbol{U}_1\boldsymbol{U}_K} = [\boldsymbol{U}_k]^K_1, \tag{11c}$$

such that the matrices $\boldsymbol{H}_k$, $\boldsymbol{V}_k$ and $\boldsymbol{U}_k$ are the $k$-th slice of the corresponding tensors $\boldsymbol{\mathcal{H}}$, $\boldsymbol{\mathcal{V}}$ and $\boldsymbol{\mathcal{U}}$, respectively.

A simple optimization problem to maximize the total SE of the system via the design of beamformers $\boldsymbol{V}_k$ and $\boldsymbol{U}_k$ subject to total TX power $P$ can then be compactly described as

$$\underset{\boldsymbol{\mathcal{V}},\boldsymbol{\mathcal{U}}}{\text{maximize}} \; f(\boldsymbol{\mathcal{V}},\boldsymbol{\mathcal{U}}|\boldsymbol{\mathcal{H}}) \triangleq \sum_{k=1}^{K} \eta_k = \eta, \tag{12a}$$

$$\text{subject to} \; \begin{cases} \sum_{k=1}^{K} \|\boldsymbol{V}_k\|_{\mathrm{F}}^2 = P \text{ in DL} \\ \|\boldsymbol{V}_k\|_{\mathrm{F}}^2 = P_k, \; \forall k \text{ in UL}, \end{cases} \tag{12b}$$

$$\|\boldsymbol{U}_k\|_{\mathrm{F}}^2 = \begin{cases} Q_k \; \forall \; k, \; \text{in DL} \\ Q_k \; \forall \; k, \; \text{in UL}, \end{cases} \tag{12c}$$

where $\eta_k$ is given by equation (6) or (10), depending on the operation mode of interest.

It is well-known that the problem described by equation (12) is not convex, due to the non-convexity of the signal-to-interference-plus-noise ratio (SINR) embedded in $\eta_k$ and the fixed power constraints. Nevertheless, considering the vast literature on methods to relax and solve non-convex [50] and in particular sum-rate optimization problems [51], the non-convexity of the functional objective $f(\boldsymbol{\mathcal{V}},\boldsymbol{\mathcal{U}}|\boldsymbol{\mathcal{H}})$ is not the greatest challenge posed by equation (12). However, a key difference between this problem and those covered in most of the literature is the fact that in equation (12), the tensor slices $\boldsymbol{H}_k$, $\boldsymbol{V}_k$ and $\boldsymbol{U}_k$ are of different sizes. Also, it should be noted that the linear coupling between $\boldsymbol{V}_k$ and $\boldsymbol{U}_k$ is another challenge that poses difficulty in solving the problem.

## III. TENSOR-BASED BF-DESIGN FOR CF-MMIMO

### A. PRELIMINARIES: STATE-OF-THE-ART BACKGROUND

Given the formulation described above and its challenges, we address in this section the design of transmit and receive BF matrices to optimize the spectral efficiency of CF-mMIMO systems.

Before we introduce our novel tensor-based mechanism, however, it is didactic to briefly review a couple of well-established BF design techniques, which will also serve as references for the performance assessment of our proposed method. To begin with, consider BF schemes based on the classic maximum ratio combiner (MRC) such as in [16], [19], which in the context hereby can be succinctly described by

$$\boldsymbol{V}_k^{\mathrm{d}} = \sum_{q=1}^{Q_k} p_{k,q} \cdot \frac{\boldsymbol{H}_k^{\mathrm{H}}}{\|\boldsymbol{H}_k^{\mathrm{H}}\|_{\mathrm{F}}} \quad \text{and} \quad \boldsymbol{U}_k^{\mathrm{d}} = \mathbf{I}_{M_k}, \tag{13a}$$

$$\boldsymbol{V}_k^{\mathrm{u}} = \sqrt{\tfrac{P_k}{M_k}} \cdot \mathbf{I}_{M_k} \text{ and } \boldsymbol{U}_k^{\mathrm{u}} = \boldsymbol{H}_k^{*}, \tag{13b}$$

where $p_{k,q}$ denotes the TX power allocated to the $q$-th stream of the $k$-th UE, which shall be addressed later, while $P$ and $P_k$ denotes the TX power available to the $k$-th UE in UL.

The MRC BF approach summarized for the DL and UL cases in equations (13) is known for its simplicity, but on the other hand has the limitation that it only maximizes the power of the desired signal without considering the effect of interference. In contrast, BF schemes based on the classic minimum mean square error (MMSE) approach aim to simultaneously maximize the desired signal power while minimizing interference [16], [17], [52], and can summarized, for the DL and UL modes respectively by

$$\boldsymbol{V}_k^{\mathrm{d}} = \sum_{q=1}^{Q_k} p_{k,q} \cdot \frac{\left(\sum_{k'} \boldsymbol{H}_{k'}^{\mathrm{H}} \boldsymbol{H}_{k'} + \sigma_k^2 \mathbf{I}_{LN}\right)^{-1} \boldsymbol{H}_k^{\mathrm{H}}}{\left\| \left(\sum_{k'} \boldsymbol{H}_{k'}^{\mathrm{H}} \boldsymbol{H}_{k'} + \sigma_k^2 \mathbf{I}_{LN}\right)^{-1} \boldsymbol{H}_k^{\mathrm{H}} \right\|_{\mathrm{F}}} \tag{14a}$$

$$\boldsymbol{U}_k^{\mathrm{d}} = \mathbf{I}_{M_k}, \tag{14b}$$

$$\boldsymbol{V}_k^{\mathrm{u}} = \sqrt{\tfrac{P_k}{M_k}} \cdot \mathbf{I}_{M_k} \tag{14c}$$

$$\boldsymbol{U}_k^{\mathrm{u}} = \boldsymbol{H}_k^{*} \left( \sum_{k'} \boldsymbol{H}_{k'}^{\mathrm{T}} \boldsymbol{H}_{k'}^{*} + \sigma_k^2 \mathbf{I}_{LN} \right)^{-1}. \tag{14d}$$

As for TX power allocation, in conventional systems this is typically resolved in either of two primary ways, depending on system priorities. The first (and also most common) is the water-filling strategy [53], which under the assumption that the effect of shadowing is negligible, such that the average power of different streams of any given UE can be considered identical, is known to maximize the sum SE and is given by

$$p_{k,q} = \frac{1}{Q_k} \sqrt{P \frac{\|\boldsymbol{H}_k\|_{\mathrm{F}}^2}{\sum_k \|\boldsymbol{H}_k\|_{\mathrm{F}}^2}}. \tag{15a}$$

The second is when fairness of resource sharing among users is also enforced, in which case TX power is allocated on the basis of channel power inversion [53], yielding

$$p_{k,q} = \frac{1}{Q_k} \sqrt{\frac{P}{\|\boldsymbol{H}_k\|_{\mathrm{F}}^2 \sum_k \frac{1}{\|\boldsymbol{H}_k\|_{\mathrm{F}}^2}}}. \tag{15b}$$

In light of the above, it can be said that despite the key difference regarding how interference is handled, the MRC and MMSE beamformers have in common – as clarified by equations (13), and (14) – the fact that both rely fundamentally on a single-sided interference mitigation, *i.e.*, precoding at the DL and receiver combining at the UL, leaving the other side merely the task of aggregating/distributing (in DL/UL, respectively) the received/transmitted signals in a manner that does not exacerbate inter-symbol interference (ISI).

Furthermore, both of these conventional linear approaches also share the limitation that inter-user interference is not mitigated in the DL, as evidenced by equations (13) and (14), since in neither scheme the BF matrix $\boldsymbol{V}_k$ towards the $k$-th user is designed with knowledge of the channels $\boldsymbol{H}_{k' \neq k}$ towards all other users. For all the above, it is fair to say that both the classic MRC and MMSE beamformers sub-utilize the antenna resources available to optimize the SE of CF-mMIMO systems; this implies that both solutions are far from being the global optimizer of equation (12), although the constraints of equations (12b) and (12c) are satisfied by both methods.

To conclude this discussion, it is worth mentioning that in the particular case of a DL MIMO system with only

two UEs, it was shown, e.g., in [35] that the pair of channel matrices $(\boldsymbol{H}_1, \boldsymbol{H}_2)$ corresponding to both users can be jointly decomposed via the GSVD, such that two mutually orthogonal subspaces, each associated with one of the users and a common mutual-interference subspace are exposed. Exploiting these features, the design of optimized TX-RX BFs is achieved [35], in particular, in the form of transmit precoders matched to the right generalized singular vectors that place the streams of each user into its own subspace, combined with the corresponding receive combiners based on unitary matrices matched to the left singular vector matrices.

Despite being a step in the right direction, solutions such as those offered in [35] are largely academic, because the practical relevance of CF-mMIMO systems with only two users is very limited; moreover, the UL BF problem is left altogether unaddressed. With the challenges associated with the optimization of the SE of CF-mMIMO as per equation (12), as well as the limitations of the classical MRC and MMSE, and with the above-described two-user solutions clarified, we next turn our attention to a state-of-the-art framework aiming to maximize the SE from an optimization perspective.

In particular, we introduce a conventional fractional programming (FP)-based BF design such as that in [54] with the aim of maximizing the total SE of the system. As considered in [54], the total SE maximization problem for a joint TX/RX BF design defined in equation (12) can be relaxed for fixed UE BFs into the following:

$$\underset{\boldsymbol{V}^{\mathrm{d}}, \boldsymbol{U}^{\mathrm{u}}}{\text{maximize}} \quad \eta \tag{16a}$$

$$\text{subject to} \quad \begin{cases} \left\|\boldsymbol{V}_k^{\mathrm{d}}\right\|_{\mathrm{F}}^2 \leq \sum_{q=1}^{Q_k} p_{k,q}, \ \forall k \\ \left\|\boldsymbol{U}_k^{\mathrm{u}}\right\|_{\mathrm{F}}^2 \leq Q_k, \ \forall k, \end{cases} \tag{16b}$$

for fixed UE BFs given by

$$\boldsymbol{U}_k^{\mathrm{d}} = \mathbf{I}_{M_k}, \tag{17a}$$

$$\boldsymbol{V}_k^{\mathrm{u}} = \sqrt{\frac{P_k}{M_k}} \cdot \mathbf{I}_{M_k}. \tag{17b}$$

Due to the logarithm of fractions, the optimization problem defined by equations (16) is non-convex, which can be efficiently convefixied through FP techniques. More specifically, one can apply the lagrangian dual transform (LDT) [54], [55] to the latter problem and transform each summation in the objective function into a relaxed variant denoted by $f_{\mathrm{LDT}}$ as in equation (18), with auxiliary variables updated as

$$\boldsymbol{\Gamma}_k^{\mathrm{d}} = \boldsymbol{V}_k^{\mathrm{d}\mathrm{H}} \boldsymbol{H}_k^{\mathrm{H}} \boldsymbol{E}_k^{\mathrm{d}^{-1}} \boldsymbol{H}_k \boldsymbol{V}_k^{\mathrm{d}}, \tag{19a}$$

$$\boldsymbol{\Gamma}_k^{\mathrm{u}} = \boldsymbol{H}_k^{*} \boldsymbol{U}_k^{\mathrm{u}\mathrm{H}} \boldsymbol{E}_k^{\mathrm{u}^{-1}} \boldsymbol{U}_k^{\mathrm{u}} \boldsymbol{H}_k^{\mathrm{T}}. \tag{19b}$$

Even though the LDT enables decoupling of the SINR from the logarithm function, the resultant objective given in equation (18), as shown at the bottom of the page is still non-convex due to the fractional terms. Following [54], making use of the quadratic transform (QT) [55] we obtain

$$\underset{\boldsymbol{V}^{\mathrm{d}}, \boldsymbol{U}^{\mathrm{u}}}{\text{maximize}} \quad \sum_{k \in \mathcal{K}} f_k^{\mathrm{QT}} \tag{20a}$$

$$\text{subject to} \quad \begin{cases} \left\|\boldsymbol{V}_k^{\mathrm{d}}\right\|_{\mathrm{F}}^2 \leq \sum_{q=1}^{Q_k} p_{k,q}, \ \forall k \\ \left\|\boldsymbol{U}_k^{\mathrm{u}}\right\|_{\mathrm{F}}^2 \leq Q_k, \ \forall k \end{cases} \tag{20b}$$

where $f_k^{\mathrm{QT}}$ is given by equation (21), as shown at the bottom of the page, and $\boldsymbol{\Psi}_k^{\mathrm{d}}$ and $\boldsymbol{\Psi}_k^{\mathrm{u}}$ denotes a newly-introduced auxiliary variable updated for fixed $\boldsymbol{V}_k^{\mathrm{d}}$ and $\boldsymbol{U}_k^{\mathrm{u}}$, respectively, according to

$$\boldsymbol{\Psi}_k^{\mathrm{d}} = \left(\sigma^2 \mathbf{I}_{M_k} + \sum_{k' \in \mathcal{K}} \boldsymbol{H}_k \boldsymbol{V}_{k'}^{\mathrm{d}} \boldsymbol{V}_{k'}^{\mathrm{d}\mathrm{H}} \boldsymbol{H}_k^{\mathrm{H}}\right)^{-1} \boldsymbol{H}_k \boldsymbol{V}_k^{\mathrm{d}}, \tag{22a}$$

$$\boldsymbol{\Psi}_k^{\mathrm{u}} = \left(\sigma^2 \boldsymbol{U}_k^{\mathrm{u}} \boldsymbol{U}_k^{\mathrm{u}\mathrm{H}} + \sum_{k' \in \mathcal{K}} \boldsymbol{U}_k^{\mathrm{u}} \boldsymbol{H}_{k'}^{\mathrm{T}} \boldsymbol{H}_{k'}^{*} \boldsymbol{U}_k^{\mathrm{u}\mathrm{H}}\right)^{-1} \boldsymbol{U}_k^{\mathrm{u}} \boldsymbol{H}_k^{\mathrm{T}}. \tag{22b}$$

According to the optimization problem defined in equation (20), we can compute tentative BF matrices by finding the root of the Lagrangian as shown in equation (23), as shown at the bottom of the next page with a Lagrangian multiplier $\mu_k \in \mathbb{R}$ optimally determined as

$$\underset{\mu_k \geq 0}{\text{minimize}} \quad \mu_k \tag{24a}$$

$$\text{subject to} \quad \begin{cases} \left\|\boldsymbol{V}_k^{\mathrm{d}}\right\|_{\mathrm{F}}^2 \leq \sum_{q=1}^{Q_k} p_{k,q} \\ \left\|\boldsymbol{U}_k^{\mathrm{u}}\right\|_{\mathrm{F}}^2 \leq Q_k \end{cases} \tag{24b}$$

which can be solved by the bisection search.

For the sake of convenience, we summarize the conventional FP-based BF design for the considered

$$f_k^{\mathrm{LDT}} = \begin{cases} \log_2\left(\det\left(\mathbf{I}_{M_k} + \boldsymbol{\Gamma}_k^{\mathrm{d}}\right)\right) - \mathrm{Tr}\left(\boldsymbol{\Gamma}_k^{\mathrm{d}}\right) - \mathrm{Tr}\left(\left(\mathbf{I}_{M_k} + \boldsymbol{\Gamma}_k^{\mathrm{d}}\right)\left(\sigma^2 \mathbf{I}_{M_k} + \boldsymbol{V}_k^{\mathrm{d}\mathrm{H}} \boldsymbol{H}_k^{\mathrm{H}} \boldsymbol{E}_k^{\mathrm{d}^{-1}} \boldsymbol{H}_k \boldsymbol{V}_k^{\mathrm{d}}\right)^{-1}\right), \text{for DL} \\ \log_2\left(\det\left(\mathbf{I}_{M_k} + \boldsymbol{\Gamma}_k^{\mathrm{u}}\right)\right) - \mathrm{Tr}\left(\boldsymbol{\Gamma}_k^{\mathrm{u}}\right) - \mathrm{Tr}\left(\left(\mathbf{I}_{M_k} + \boldsymbol{\Gamma}_k^{\mathrm{u}}\right)\left(\sigma^2 \boldsymbol{U}_k^{\mathrm{u}} \boldsymbol{U}_k^{\mathrm{u}\mathrm{H}} + \boldsymbol{H}_k^{*} \boldsymbol{U}_k^{\mathrm{u}\mathrm{H}} \boldsymbol{E}_k^{\mathrm{u}^{-1}} \boldsymbol{U}_k^{\mathrm{u}} \boldsymbol{H}_k^{\mathrm{T}}\right)^{-1}\right), \text{for UL} \end{cases} \tag{18}$$

$$f_k^{\mathrm{QT}} = \begin{cases} \log_2\left(\det\left(\mathbf{I}_{M_k} + \boldsymbol{\Gamma}_k^{\mathrm{d}}\right)\right) - \mathrm{Tr}\left(\boldsymbol{\Gamma}_k^{\mathrm{d}}\right) + \mathrm{Tr}\left(\left(\mathbf{I}_{M_k} + \boldsymbol{\Gamma}_k^{\mathrm{d}}\right)\left(2\Re\left[\boldsymbol{\Psi}_k^{\mathrm{d}\mathrm{H}} \boldsymbol{H}_k \boldsymbol{V}_k^{\mathrm{d}}\right] - \boldsymbol{\Psi}_k^{\mathrm{d}\mathrm{H}}\left\{\sigma^2 \mathbf{I}_{M_k} + \sum_{k' \in \mathcal{K}} \boldsymbol{H}_k \boldsymbol{V}_{k'}^{\mathrm{d}} \boldsymbol{V}_{k'}^{\mathrm{d}\mathrm{H}} \boldsymbol{H}_k^{\mathrm{H}}\right\} \boldsymbol{\Psi}_k^{\mathrm{d}}\right)\right), \text{for DL} \\ \log_2\left(\det\left(\mathbf{I}_{M_k} + \boldsymbol{\Gamma}_k^{\mathrm{u}}\right)\right) - \mathrm{Tr}\left(\boldsymbol{\Gamma}_k^{\mathrm{u}}\right) + \mathrm{Tr}\left(\left(\mathbf{I}_{M_k} + \boldsymbol{\Gamma}_k^{\mathrm{u}}\right)\left(2\Re\left[\boldsymbol{\Psi}_k^{\mathrm{u}\mathrm{H}} \boldsymbol{U}_k^{\mathrm{u}} \boldsymbol{H}_k^{\mathrm{T}}\right] - \boldsymbol{\Psi}_k^{\mathrm{u}\mathrm{H}}\left\{\sigma^2 \boldsymbol{U}_k^{\mathrm{u}} \boldsymbol{U}_k^{\mathrm{u}\mathrm{H}} + \sum_{k' \in \mathcal{K}} \boldsymbol{U}_k^{\mathrm{u}} \boldsymbol{H}_{k'}^{\mathrm{T}} \boldsymbol{H}_{k'}^{*} \boldsymbol{U}_k^{\mathrm{u}\mathrm{H}}\right\} \boldsymbol{\Psi}_k^{\mathrm{u}}\right)\right), \text{for UL} \end{cases} \tag{21}$$

**Algorithm 1** CONVENTIONAL FP-BASED BF

**Input:** Channel tensor $\mathcal{H}$.
**Output:** BF tensors $\mathcal{U}$ or $\mathcal{V}$.

1: Initialize BF with MMSE as in equations (14), and (15);
2: **while** Convergence criteria are not satisfied **do**
3: Update $\mathbf{\Gamma}_k, \forall k$ as in equation (19);
4: Update $\mathbf{\Psi}_k, \forall k$ as in equation (22);
5: Bisection search of $\mu_k, \forall k$ as equations (24) and (23);
6: Update $\boldsymbol{V}'_k$ or $\boldsymbol{U}'_k$ as in equation (23);
7: **end while**
8: Collect $\boldsymbol{V}'_k$ into $\mathcal{V}$ as in equation (11b), and $\boldsymbol{U}'_k$ into $\mathcal{U}$ as in equation (11c), respectively.

user-heterogeneous CF-mMIMO systems in Algorithm 1 with convergence criteria

$$\sum_k \left\|\boldsymbol{V}'_k - \boldsymbol{V}_k\right\|_{\mathrm{F}}^2 / \sum_k \left\|\boldsymbol{V}'_k\right\|_{\mathrm{F}}^2 < 10^{-8}, \tag{25a}$$

$$\sum_k \left\|\boldsymbol{U}'_k - \boldsymbol{U}_k\right\|_{\mathrm{F}}^2 / \sum_k \left\|\boldsymbol{U}'_k\right\|_{\mathrm{F}}^2 < 10^{-8}, \tag{25b}$$

such that the algorithm is terminated when either of them is triggered.

### B. TENSOR DECOMPOSITION FRAMEWORK

We seek a CF-mMIMO BF mechanism in which:

- Each UE can be equipped with any number of antennas;
- All the available spatial resources are exploited via design of joint TX/RX BF;
- No restriction on the number of users is imposed;
- Both ISI and multi-user interference (MUI) are mitigated.

To that end, consider the DL complex baseband signal model of equation (5), which after incorporating the SVD of the channel matrix $\boldsymbol{H}_k$ becomes

$$\boldsymbol{y}_k = \boldsymbol{U}_k^{\mathrm{d}} \underbrace{\boldsymbol{B}_k \mathbf{\Sigma}_k \boldsymbol{A}_k^{\mathrm{T}}}_{=\boldsymbol{H}_k} \boldsymbol{V}_k^{\mathrm{d}} \boldsymbol{s}_k + \sum_{k'=1, k' \neq k}^{K} \boldsymbol{U}_k^{\mathrm{d}} \underbrace{\boldsymbol{B}_k \mathbf{\Sigma}_k \boldsymbol{A}_k^{\mathrm{T}}}_{=\boldsymbol{H}_k} \boldsymbol{V}_{k'}^{\mathrm{d}} \boldsymbol{s}_{k'} + \boldsymbol{U}_k^{\mathrm{d}} \boldsymbol{n}_k, \tag{26}$$

where the right and left singular vectors of $\boldsymbol{H}_k$ are given by the matrices[1] $\boldsymbol{A}_k^*$ and $\boldsymbol{B}_k$, while the corresponding singular values are in the diagonal entries of the diagonal matrix $\mathbf{\Sigma}_k$.

As evidenced by the terms $\boldsymbol{A}_k^{\mathrm{T}} \boldsymbol{V}_{k'}$ with $k' \neq k$ in equation (26), performing the SVD of each channel matrix $\boldsymbol{H}_k$ separately cannot yield a BF strategy in which MUI is effectively mitigated. Instead, it is clear that the problem requires the channel matrices $\boldsymbol{H}_k$ to be processed collectively, or in other words, a tensor decomposition of the tensor $\mathcal{H}$.

1. We highlight the slightly unusual definition of the right singular matrix, which is adopted here for future convenience.

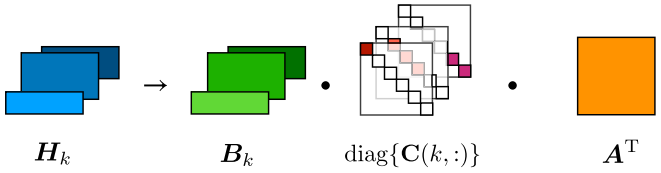


**FIGURE 2.** Illustration of OEML-GSVD.

Although many methods to decompose tensors exist [38], [39], [41], [56], we develop our own variation of the technique referred to as the ML-GSVD recently proposed in [42] and illustrated in Figure 2, in which each $k$-th slice $\boldsymbol{H}_k$ of the tensor $\mathcal{H}$ is decomposed into

$$\boldsymbol{H}_k = \boldsymbol{B}_k \overbrace{\mathrm{diag}\left\{\langle \mathbf{C}^{\mathrm{T}} \rangle_k\right\}}^{\triangleq \mathbf{C}_k} \boldsymbol{A}^{\mathrm{T}}, \tag{27}$$

where $\langle \boldsymbol{X} \rangle_k$ denotes the $k$-th column of the matrix $\boldsymbol{X}$, $\boldsymbol{B}_k \in \mathbb{C}^{M_k \times LN}$, with $\boldsymbol{B}_k \boldsymbol{B}_k^{\mathrm{H}} = \mathbf{I}_{M_k}$ is a unitary matrix akin to the left singular vectors in a conventional SVD, $\boldsymbol{A} \in \mathbb{C}^{LN \times LN}$ is a square matrix also similar to the right singular vectors of a conventional SVD except for the fundamental difference that it is common to all slices of $\mathcal{H}$, and $\mathbf{C} \in [0, 1]^{K \times LN}$ is a binary block diagonal matrix, such that the $k$-th row of $\mathbf{C}$ is used to construct the diagonal matrix $\mathbf{C}_k \in \mathbb{C}^{LN \times LN}$.

At this point it is important to remark that, in light of the transpose relationship between the effective DL and UL channel matrices as described by the definition of $\boldsymbol{H}_k^{\mathrm{u}}$, the tensor decomposition of channel tensor $\mathcal{H}$ as given in equation (27) can be exploited both by DL and UL beamformers, as discussed later in Section III-C.

Therefore, our motivation continues to be the tensor decomposition of $\mathcal{H}$ with a focus on the DL case, but without loss of generality. From equation (27), the complex baseband signal model can be written as

$$\boldsymbol{y}_k = \boldsymbol{U}_k^{\mathrm{d}} \boldsymbol{B}_k \mathbf{C}_k \boldsymbol{A}^{\mathrm{T}} \boldsymbol{V}_k^{\mathrm{d}} \boldsymbol{s}_k + \sum_{k'=1, k' \neq k}^{K} \boldsymbol{U}_k^{\mathrm{d}} \boldsymbol{B}_k \mathbf{C}_k \boldsymbol{A}^{\mathrm{T}} \boldsymbol{V}_{k'}^{\mathrm{d}} \boldsymbol{s}_{k'} + \boldsymbol{U}_k^{\mathrm{d}} \boldsymbol{n}_k. \tag{28}$$

Before we proceed to describing the algorithm here proposed to construct the decomposition described by equation (27), let us highlight the role and key property of each of the component matrices, bearing in mind the intended application to the BF design of CF-mMIMO systems.

$$\boldsymbol{V}_k^{\mathrm{d}} = \left(\mu_k^{\mathrm{d}} \mathbf{I}_{LN} + \sum_{k' \in \mathcal{K}} \boldsymbol{H}_{k'}^{\mathrm{H}} \mathbf{\Psi}_{k'}^{\mathrm{d}} (\mathbf{I}_{M_{k'}} + \mathbf{\Gamma}_{k'}^{\mathrm{d}}) \mathbf{\Psi}_{k'}^{\mathrm{d}^{\mathrm{H}}} \boldsymbol{H}_{k'}\right)^{-1} \boldsymbol{H}_k^{\mathrm{H}} \mathbf{\Psi}_k^{\mathrm{d}} \left(\mathbf{I}_{M_k} + \mathbf{\Gamma}_k^{\mathrm{d}}\right) \tag{23a}$$

$$\mathrm{vec}\left(\boldsymbol{U}_k^{\mathrm{u}}\right) = \left(\mu_k^{\mathrm{u}} \mathbf{I}_{LNM_k} + \left(\sigma^2 \mathbf{I}_{LN} + \sum_{k' \in \mathcal{K}} \boldsymbol{H}_{k'}^{\mathrm{H}} \boldsymbol{H}_{k'}\right) \otimes \mathbf{\Psi}_k^{\mathrm{u}} (\mathbf{I}_{M_k} + \mathbf{\Gamma}_k^{\mathrm{u}}) \mathbf{\Psi}_k^{\mathrm{u}^{\mathrm{H}}}\right)^{-1} \cdot \mathrm{vec}\left(\mathbf{\Psi}_k^{\mathrm{u}} \left(\mathbf{I}_{M_k} + \mathbf{\Gamma}_k^{\mathrm{d}}\right) \boldsymbol{H}_k^*\right) \tag{23b}$$

Starting with the common matrix $\boldsymbol{A}$, it is evident from equation (28) that the purpose of the DL TX beamformer is to orthogonalize the transmission over the channel tensor, by assigning each transmit symbol vector $\boldsymbol{s}_{k'}$ to a dedicated subspace of the common matrix $\boldsymbol{A}$, so as to mitigate MUI.

In other words, it is desired that each TX-BF matrix $\boldsymbol{V}_k \in \mathbb{C}^{LN\times Q_k}$ be aligned with the common matrix $\boldsymbol{A}$. In turn, the binary matrix $\mathbf{C}$ must be such that only the entries of its $k$-th row associated with the private subspace of the $k$-th user, only the corresponding diagonal entries of the matrix $\mathbf{C}_k$ – are non-zero. Altogether, it is desired that any given $j$-th column of $\mathbf{C}$ has only one non-zero element (set to 1), and if such unit entry occurs at the $k$-th row, then it can be said that the $j$-th one-dimensional subspace of the channel tensor $\boldsymbol{\mathcal{H}}$ is private to the $k$-th UE.

We again highlight a fundamental difference between the tensor decomposition introduced here and the ML-GSVD method proposed in [42], which is the fact that in the ML-GSVD of [42] the entries of the matrix $\mathbf{C}$ are not binary. Furthermore, we note that the orthogonal separation of all subspaces in the channel tensor $\boldsymbol{\mathcal{H}}$ (*i.e.*, interference-free decomposition) is only possible if $LN \geq \sum_k Q_k$, with $Q_k \leq M_k$, $\forall\, k$. In turn, in case $LN < \sum_k Q_k$ or $Q_k > M_k$ for some $k$, it follows that some subspaces of $\boldsymbol{\mathcal{H}}$ will be overlapped or shared by the corresponding UEs. Such shared subspaces are referred to as common subspaces.

With these objectives clarified, we follow [41] and initialize $\boldsymbol{A}$ and $\mathbf{C}$ as the left singular matrix of $\sum_{k=1}^{K} \boldsymbol{H}_k^{\mathrm{H}}\boldsymbol{H}_k$ and $\mathbf{C}$ as a random matrix with entries taken randomly and uniformly from the interval [0, 1]. In other words, if we denote the initial $\boldsymbol{A}$ and $\mathbf{C}$ respectively by $\boldsymbol{A}^{(0)}$ and $\mathbf{C}^{(0)}$, then

$$\boldsymbol{A}^{(0)} = \boldsymbol{X} \text{ with } \boldsymbol{X}\boldsymbol{\Sigma}\boldsymbol{X}^{\mathrm{H}} = \sum_{k=1}^{K} \boldsymbol{H}_k^{\mathrm{H}}\boldsymbol{H}_k, \tag{29}$$

$$\mathbf{C}^{(0)} = \left[c_{n,m}^{(0)}\right]_{1,1}^{LN,LN} \text{ with } c_{n,m}^{(0)} \sim \mathcal{U}(0,1), \tag{30}$$

where $\mathcal{U}(0, 1)$ denotes the uniform distribution in the interval [0, 1] and $(n, m) \in \{1, \ldots, LN\}$.

In possession of a so-initialized pair of matrices $\boldsymbol{A}^{(0)}$ and $\mathbf{C}^{(0)}$, and anticipating that both will be subsequently updated such that their construction at the $i$-th iteration are similarly denoted by $\boldsymbol{A}^{(i)}$ and $\mathbf{C}^{(i)}$, respectively, the corresponding $i$-th construction of the matrices $\boldsymbol{B}_k$ can be obtained as follows.

First, consider the linear equation

$$\boldsymbol{H}_k = \overbrace{\boldsymbol{B}_k^{(i)}\underbrace{\mathbf{C}_k^{(i)}\boldsymbol{A}^{(i)\mathrm{T}}}_{\triangleq \boldsymbol{D}_k^{(i)}}}^{\triangleq \hat{\boldsymbol{H}}_k^{(i)}} + \boldsymbol{W}_k^{(i)}, \tag{31}$$

where $\boldsymbol{W}_k^{(i)} \in \mathbb{C}^{M_k\times LN}$ denotes a fitting error matrix and we have implicitly defined the auxiliary matrices $\hat{\boldsymbol{H}}_k^{(i)}$ and $\boldsymbol{D}_k^{(i)}$, such that in the future we may also define the tensor

$$\hat{\boldsymbol{\mathcal{H}}} \triangleq \left[\!\!\left[\hat{\boldsymbol{H}}_1, \hat{\boldsymbol{H}}_2, \hat{\boldsymbol{H}}_K\right]\!\!\right] = \left[\hat{\boldsymbol{H}}_k\right]_1^K, \tag{32}$$

Having clearly highlighted that the matrices $\boldsymbol{A}^{(i)}$, $\boldsymbol{B}_k^{(i)}$ and $\mathbf{C}_k^{(i)}$ are to be updated iteratively, for the sake of notational simplicity we omit hereafter the super index $^{(i)}$ whenever unnecessary.

Given equation (31), the following direct fitting problem constrained by the unitarity of $\boldsymbol{B}_k$ can be formulated:

$$\boldsymbol{B}_k = \underset{\boldsymbol{B}_k}{\operatorname{argmin}}\ \mathrm{Tr}\big(\boldsymbol{W}_k\boldsymbol{W}_k^{\mathrm{H}}\big) \text{ subject to } \boldsymbol{B}_k\boldsymbol{B}_k^{\mathrm{H}} = \mathbf{I}_{M_k}, \tag{33}$$

which readily yields the Lagrangian,

$$\mathcal{L} = \mathrm{Tr}\big(\boldsymbol{W}_k\boldsymbol{W}_k^{\mathrm{H}}\big) + \mathrm{Tr}\big(\boldsymbol{L}_{\mathrm{m}}\big(\boldsymbol{B}_k\boldsymbol{B}_k^{\mathrm{H}} - \mathbf{I}_{M_k}\big)\big), \tag{34}$$

where $\boldsymbol{W}_k = \boldsymbol{H}_k - \boldsymbol{B}_k\boldsymbol{D}_k$ and $\boldsymbol{L}_{\mathrm{m}} \in \mathbb{C}^{M_k\times M_k}$ denotes the Lagrange multiplier matrix.

By virtue of Wirtinger calculus, a closed-form solution to equation (33) can be given by [57],

$$\boldsymbol{B}_k^{(i)} = \boldsymbol{H}_k\boldsymbol{D}_k^{\mathrm{H}}\big(\boldsymbol{D}_k\boldsymbol{H}_k^{\mathrm{H}}\boldsymbol{H}_k\boldsymbol{D}_k^{\mathrm{H}}\big)^{-\frac{1}{2}}. \tag{35}$$

It will prove convenient to define the tensor

$$\boldsymbol{\mathcal{B}} \triangleq \left[\!\!\left[\boldsymbol{B}_1, \boldsymbol{B}_2, \boldsymbol{B}_K\right]\!\!\right] = [\boldsymbol{B}_k]_1^K, \tag{36}$$

which collects all the $K$ matrices $\boldsymbol{B}_k$.

Once a new update of $\boldsymbol{B}_k$ is obtained from equation (35), $\mathbf{C}$ needs to be updated for a fixed $\boldsymbol{B}_k$ and $\boldsymbol{A}$. In the ML-GSVD algorithm proposed in [42], the update rule of $\mathbf{C}$ is given by

$$\mathbf{C} = \boldsymbol{\mathcal{D}}_{(3)}\left(\mathrm{diag}\left\{\frac{1}{\|\langle\boldsymbol{A}\rangle_1\|_2^2}, \ldots, \frac{1}{\|\langle\boldsymbol{A}\rangle_{LN}\|_2^2}\right\}(\boldsymbol{A}\diamond\mathbf{I}_{LN})^{\mathrm{H}}\right)^{\mathrm{T}}, \tag{37}$$

where $\diamond$ denotes the row-wise Khatri-Rao tensor product such that $\left[\begin{smallmatrix} a & b \\ c & d \end{smallmatrix}\right] \diamond \left[\begin{smallmatrix} 1 & 0 \\ 0 & 1 \end{smallmatrix}\right] = \left[\begin{smallmatrix} a & 0 & c & 0 \\ 0 & b & 0 & d \end{smallmatrix}\right]^{\mathrm{T}}$, and $\boldsymbol{\mathcal{D}}_{(3)}$ is the third mode unfolding [37] of the tensor $\boldsymbol{\mathcal{D}}$, defined[2] as

$$\boldsymbol{\mathcal{D}} \triangleq \left[\!\!\left[\boldsymbol{D}_1^{\mathrm{T}}, \boldsymbol{D}_2^{\mathrm{T}}, \boldsymbol{D}_K^{\mathrm{T}}\right]\!\!\right] = \left[\boldsymbol{D}_k^{\mathrm{T}}\right]_1^K. \tag{38}$$

Notice, however, that the update rule given by equation (37) allows for $\mathbf{C}$ to be complex-valued, while here it is desired that $\mathbf{C}$ is binary. Departing from [42], we therefore introduce the following additional updates onto the matrices $\boldsymbol{A}$ and $\mathbf{C}$

$$\langle\boldsymbol{A}\rangle_{\ell_n} = |\langle\mathbf{C}\rangle_{\ell_n}|\langle\boldsymbol{A}\rangle_{\ell_n}, \tag{39}$$

$$\langle\mathbf{C}^{(i)}\rangle_{\ell_n} = \frac{\big|\langle\mathbf{C}\rangle_{\ell_n}\big|}{\max(|\langle\mathbf{C}\rangle_{\ell_n}|, \varepsilon)}, \tag{40}$$

where $\ell_n \in \{1, \ldots, LN\}$, $|\cdot|$ denotes element-wise absolute value and $0 < \varepsilon \ll 1$. In plain words, by means of equation (39) any scaling effect (related to the channel power) contained in $\mathbf{C}$ is moved to $\boldsymbol{A}$, while by means of equation (40) all entries of $\mathbf{C}$ are projected onto the domain (0, 1).

Next, we invoke the dimension theorem [58] and recall equation (27) to argue that it is sufficient that only up to $M_k$

elements of each $k$-th row $\langle \mathbf{C}^{\mathrm{T}} \rangle_k$ of $\mathbf{C}$ – or equivalently only $M_k$ diagonal elements of $\mathbf{C}_k$ – are nonzero in order for the decomposition of $\boldsymbol{H}_k$ to be as in equation (27). Consequently, we project the entries of $\mathbf{C}$ onto the binary domain as follows.

Define the sets $\mathcal{Z}_k$ which collect, for each $k$-th row of $\mathbf{C}$, the indices of its smallest $LN - M_k$ elements. Then we set

$$c^{(i)}_{k,\ell_n} = 0, \forall \ell_n \in \mathcal{Z}_k. \tag{41}$$

We remark that especially in the case when $LN < \sum_k M_k$, which corresponds to an "overloaded" system in the sense that the degrees of freedom available at the receiver is lower than the total degrees of freedom of the collection of transmitters, equations (40) and (41) play a significant role in separating the spaces allocated to different UE, with important consequences in the application of the tensor decomposition to TX/RX BF in CF-mMIMO systems.

In particular, as a consequence of these projections, a pressure is created within the construction of $\mathbf{C}_k$ to allocate to a given user its subspaces with the largest singular values. Specifically, if two users $k$ and $k'$ are such that $c_{k,\ell_n} \gg c_{k',\ell_n}$, the tendency is for equations (40) and (41) to produce $c_{k,\ell_n} \to 1$ and $c_{k',\ell_n} \to 0$, even in overloaded conditions. It is this feature that motivates us to dub the tensor decomposition here presented the orthogonality-enforcing ML-GSVD (OEML-GSVD), although it must be clear to the reader that in the overloaded case orthogonality cannot be ensured, such that occasionally overlapped subspaces will result, which must then be orthogonalized by means of an orthogonal resource allocation scheme which, in the context of this article, is part of the BF methods described in the next subsection.

In turn, in underloaded conditions that are of interest in this article, *i.e.*, if $LN \geq \sum_k M_k$, the projection enforced by equation (41) may cause some $k$-th rows of $\mathbf{C}$ not to have the same number of non-zero elements as $M_k$. In order to avoid this underutilization of available spatial resources and take full advantage of the degree of freedom (DoF) of $\boldsymbol{\mathcal{H}}$, the following projection is applied to $\mathbf{C}$ if and only if $LN \geq \sum_k M_k$. To that end, the set $\mathcal{F}$ of free dimensions is first constructed, defined as

$$\mathcal{F} \triangleq \left\{ \ell_n \middle| \|\langle \mathbf{C} \rangle_{\ell_n}\|_1 = 0, \ \forall \ \ell_n \in \{1, \ldots, LN\} \right\}. \tag{42}$$

Next, $\mathcal{F}$ is randomly partitioned into $K$ mutually-exclusive subsets $\mathcal{F}_k$, each with cardinality $|\mathcal{F}_k| = M_k - \|\langle \mathbf{C}^{\mathrm{T}} \rangle_k\|_1$ such that

$$\mathcal{F}_k \cap \mathcal{F}_{k'} = \left\{ \forall \ (k, k') | k \neq k', \ \bigcup_{k=1}^{K} \mathcal{F}_k \subset \mathcal{F} \right\}. \tag{43}$$

Then, the subspaces in $\mathcal{F}_k$ are allocated to the $k$-th user, *i.e.*,

$$c^{(i)}_{k,\ell_n} = 1, \forall \ \ell_n \in \mathcal{F}_k, \ \forall \ k. \tag{44}$$

2. We call attention to the fact that, for convenience, the tensor $\boldsymbol{\mathcal{D}}$ is defined based on the transposes of the matrices $\boldsymbol{D}_k$, therefore differing from the definitions of other tensors given in equations (11).

**Algorithm 2** ORTHOGONALITY-ENFORCING ML-GSVD

**Choice Parameters:** $\epsilon$, $\delta$, $\xi$, $\omega_{\max}$ sufficiently small, and $i_{\max}$ sufficiently large.
**Input:** $\boldsymbol{\mathcal{H}} \in \mathbb{C}^{K \times M_k \times LN}$
**Output:** $\boldsymbol{B}_k \in \mathbb{C}^{M_k \times LN}$, $\mathbf{C} \in \{0, 1\}^{LN \times LN}$, $\boldsymbol{A} \in \mathbb{C}^{LN \times LN}$

Initialize $\boldsymbol{A}$ and $\mathbf{C}$ as in equations (29) and (30);
**while** $\|\boldsymbol{\mathcal{H}} - \hat{\boldsymbol{\mathcal{H}}}\|^2 / \|\boldsymbol{\mathcal{H}}\|^2 > \omega_{\max}$ or $i \leq i_{\max}$ **do**
  **for** $k = 1, 2, ..., K$ **do**
    Construct $\boldsymbol{B}_k$ as in equation (35);
  **end for**
  Update $\mathbf{C}$ as in equations (37), (40) and (41);
  **if** $LN \geq \sum_k M_k$ **then**
    Update $\mathbf{C}$ further as in equation (44);
  **end if**
  Update $\boldsymbol{A}$ as in equaiton (45)
  Increment iteration counter $i \leftarrow i + 1$;
**end while**

In possession of the latest updates of $\mathbf{B}_k$ as per equation (35), and of all entries of $\mathbf{C}$ as per equations (40), (41), and (44) (when applicable), the final update of the common generalized right singular matrix $\boldsymbol{A}$ is obtained as

$$\boldsymbol{A}^{(i)T} = \boldsymbol{\mathcal{D}}_{(1)} \mathrm{blkdiag} \left\{ \frac{\langle \mathbf{C} \rangle_1^{\mathrm{H}}}{\|\langle \mathbf{C} \rangle_1\|_2^2 + \delta}, \ldots, \frac{\langle \mathbf{C} \rangle_{LN}^{\mathrm{H}}}{\|\langle \mathbf{C} \rangle_{LN}\|_2^2 + \delta} \right\} + \xi \mathbf{I}_{LN}, \tag{45}$$

where $\boldsymbol{\mathcal{D}}_{(1)}$ denotes the first mode unfolding [37] of the tensor $\boldsymbol{\mathcal{D}}$, and $\delta$ and $\xi$ are sufficiently small quantities inserted to avoid divergent ratios and ensure the full-rankness of $\boldsymbol{A}$, respectively.

The updates given in equations (35)–(45) are repeatedly computed until the solution converges. In allusion to the feature that private subspaces are allocated to each UE, thus ensuring their orthogonality as long as $LN \geq \sum_k M_k$, while also creating a "pressure" for all subspaces to be private even when $LN < \sum_k M_k$, unlike the method proposed in [42], we refer to our tensor decomposition described in this subsection as the Orthogonality Enforcing ML-GSVD, which for convenience is presented as pseudo-code in Algorithm 2.

### C. BEAMFORMING DESIGN

Similar to the SVD-based point-to-point MIMO BF design, our goal is to take advantage of the tensor decomposition described above in order to enable interference-free communications even in multi-user MIMO scenarios.

In case the total spatial degree is larger than the total number of UE antennas (*i.e.*, $LN \geq \sum_k M_k$), we ensure $Q_k = M_k$ for all $k$ UEs, while in case of $LN < \sum_k M_k$, we resort to $Q_k \leq M_k$ streams, with $LN = \sum_k Q_k$.[3] In other words, in what follows TX and RX BF matrices will be designed such that each $k$-th user can receive $Q_k$ streams free of ISI and MUI, to which it suffices that $\boldsymbol{V}_k \in \mathbb{C}^{LN \times Q_k}$.

With these remarks in mind, and as illustrated in Figure 3, the BF strategy is to exploit and complement the orthogonality enforcing feature of the OEML-GSVD-based tensor

3. Although this case is outside the scope of this article, for the sake of completeness, the proposed algorithm is presented for general conditions including the case $LN < \sum_k M_k$.

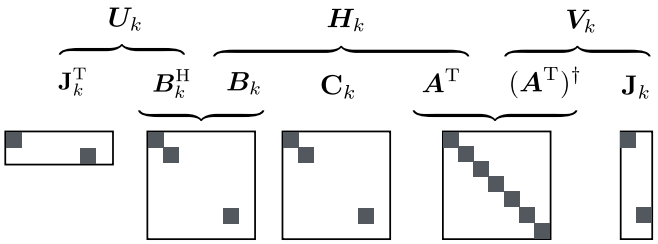


**FIGURE 3.** Illustration of Orthogonality Enforcing ML-GSVD-based beamformer.

decomposition described in the preceding subsection as follows.

On the transmitter side, each TX BF matrix $\boldsymbol{V}_k$ should both diagonalize the common right singular matrix $\boldsymbol{A}$, and select from it a subspace of dimension $Q_k$ that best fits the $k$-th UE, in accordance with the corresponding non-zero diagonal entries of $\mathbf{C}_k$. Before we proceed, it is worth noting that although $\boldsymbol{A}$ is in theory always invertible, occasionally ill-conditioning might arise due to numerical issues. To circumvent that problem, the pseudo-inverse adopted hereafter will be taken as the capped pseudo-inverse, whose construction is described as follows.

Consider the singular value decomposition $\boldsymbol{A} = \boldsymbol{W}_{\mathrm{L}} \Lambda \boldsymbol{W}_{\mathrm{R}}^{\mathrm{H}}$ and let $\bar{\Lambda}$ be the capped singular value matrix given by

$$\bar{\Lambda} \triangleq \mathrm{diag}(\max(\mathrm{diag}(\Lambda), \kappa \mathbf{1}_{LN\times 1})), \tag{46}$$

in which $\kappa$ denotes a small constant.

Then, the capped pseudo-inverse of $\boldsymbol{A}$ is defined as

$$\boldsymbol{A}^{\dagger} \triangleq \boldsymbol{W}_{\mathrm{R}} \bar{\Lambda}^{-1} \boldsymbol{W}_{\mathrm{L}}^{\mathrm{H}}. \tag{47}$$

Hence, the $q$-th column of the DL/UL TX BF matrices corresponding to the $k$-th user can be designed as

$$\langle \boldsymbol{V}_k^{\mathrm{d}} \rangle_q = p_{k,q} \frac{\left(\boldsymbol{A}^{\mathrm{T}}\right)^{\dagger} \langle \mathbf{J}_k \rangle_q}{\left\| \left(\boldsymbol{A}^{\mathrm{T}}\right)^{\dagger} \langle \mathbf{J}_k \rangle_q \right\|_{\mathrm{F}}} \text{ for } q \in \{1, 2, \ldots, Q_k\}, \tag{48a}$$

$$\langle \boldsymbol{V}_k^{\mathrm{u}} \rangle_q = p_{k,q} \frac{\boldsymbol{B}_k^{*} \langle \mathbf{J}_k \rangle_q}{\left\| \boldsymbol{B}_k^{*} \langle \mathbf{J}_k \rangle_q \right\|_{\mathrm{F}}} \text{ for } q \in \{1, 2, \ldots, Q_k\}, \tag{48b}$$

where $p_{k,q}$ denotes the allocated TX power to the $q$-th stream of the $k$-th UE and the subspace selection matrix $\mathbf{J}_k$ is designed such that an orthogonal subspace of dimension $Q_k$ is allocated to the $k$-th user.

The construction of the subspace selection matrix $\mathbf{J}_k$ depends on the loading conditions. In general, the $\ell_n$-row of the $q$-th column of $\mathbf{J}_k$ denoted $j_{k_{\ell_n,q}}$ is defined in binary and if the $\ell_n$-th resource is allocated to the $q$-th dimension of the $k$-th user, their value is 1, otherwise it is 0.

$$j_{k_{\ell_n,q}} = \begin{cases} 1 & \text{allocated} \\ 0 & \text{otherwise,} \end{cases} \tag{49}$$

with $\ell_n = \{1, \ldots, LN\}$.

In case $LN \geq \sum_k Q_k$, the OEML-GSVD described above yields a block diagonal matrix $\mathbf{C}$ with $\|\langle \mathbf{C}^{\mathrm{T}} \rangle_k\|_1 = Q_k, \ \forall\, k$ and $\|\langle \mathbf{C} \rangle_{\ell_n}\|_1 \leq 1, \ \forall\, \ell_n$. In other words, in this case all subspaces constructed via the OEML-GSVD are private, such that $\mathbf{J}_k$ is then given simply by the $Q_k$ non-zero columns of $\mathbf{C}_k$. Defining then the operator $\mathsf{P}[\,\cdot\,]$ that punctures out all zero column vectors of a matrix, we can compactly express $\mathbf{J}_k$ in the underloaded and fully-loaded cases as

$$\mathbf{J}_k = \mathsf{P}[\mathbf{C}_k]. \tag{50}$$

In turn, in case $LN < \sum_k Q_k$, the total spatial DoFs available are insufficient to allocate to all users private subspaces of dimensions $Q_k$, such that the OEML-GSVD yields a matrix $\mathbf{C}$ with $\|\langle \mathbf{C} \rangle_{\ell_n}\|_1 > 1$ for some dimensions $\ell_n$. For future convenience, let us then define the set $\mathcal{S}$ of shared dimensions

$$\mathcal{S} \triangleq \left\{ \ell_n \middle| \|\langle \mathbf{C} \rangle_{\ell_n}\|_1 > 1, \ \forall\, \ell_n \in \{1, \ldots, LN\} \right\}. \tag{51}$$

The orthogonal allocation of shared dimensions in the BF problem here studied is similar to the subcarrier allocation problem in multiuser orthogonal frequency-division multiple access (OFDMA) systems, and can be achieved through different strategies. For example, in order to maximize the sum SE, the indices in $\mathcal{S}$ can be allocated one by one in a greedy fashion, such that each dimension from $\mathcal{S}$ is allocated to the user that results in the largest increase in $\sum_k \eta_k$ in [59], until all users have their private subspace with dimension $Q_k$. For simplicity of reference, we shall denote this allocation as

$$\mathcal{S} \underset{\text{greedy}}{\rightarrow} \left\{ \mathcal{Q}_1^{\mathrm{G}}, \ldots, \mathcal{Q}_K^{\mathrm{G}} \right\}, \tag{52a}$$

with $\bigcup_{k=1}^{K} \mathcal{Q}_k^{\mathrm{G}} = \mathcal{S}$, and where $\mathcal{Q}_k^{\mathrm{G}}$ denotes the set of indices from $\mathcal{S}$ allocated to the $k$-th user under a greedy strategy.

Alternatively, a fairness-aware strategy is also possible, in which the minimum SE over all UEs is maximized, and for which a low-complexity near-optimal scheme exists [60] in the context of subcarrier allocation in OFDMA systems. In similarity with the above, we denote this allocation as

$$\mathcal{S} \underset{\text{fair}}{\rightarrow} \left\{ \mathcal{Q}_1^{\mathrm{F}}, \ldots, \mathcal{Q}_K^{\mathrm{F}} \right\}, \tag{52b}$$

where $\mathcal{Q}_k^{\mathrm{F}}$ denotes the set of indices from $\mathcal{S}$ allocated exclusively to the $k$-th user under a fairness-aware strategy.

Once the orthogonal allocation of the shared spaces to all users is completed following equation (52a) or (52b), as desired, the corresponding selection matrix for all users can be obtained by appending the allocated subspaces to the private subspaces; this can be expressed as

$$\mathbf{J}_k = \left[ \mathsf{P}[\mathbf{C}_k], \langle \mathbf{C}_k \rangle_{q \in \mathcal{Q}_k} \right], \tag{53}$$

where in the latter equation $\mathcal{Q}_k$ may be interpreted as $\mathcal{Q}_k^{\mathrm{G}}$ or $\mathcal{Q}_k^{\mathrm{F}}$, depending on the optimization criterion followed.

Turning our attention to the receiver, as illustrated in Figure 3, the DL RX BF strategy is used for the matrices $\boldsymbol{U}_k$ to diagonalize the left RX unitary matrix $\boldsymbol{B}_k$ of the channel tensor and to match the private subspace assignment performed at the transmitter, such that we can write concisely

$$\boldsymbol{U}_k^{\mathrm{d}} = \mathbf{J}_k^{\mathrm{T}} \boldsymbol{B}_k^{\mathrm{H}}. \tag{54a}$$

**Algorithm 3** OEML-GSVD-BASED BF

**Choice Parameters:** Singular value cap $\kappa$
**Input:** OEML-GSVD decomposed tensor $\boldsymbol{\mathcal{H}}$ in the form of $\boldsymbol{\mathcal{B}}$, $\mathbf{C}$ and $\boldsymbol{A}$.
**Output:** BF tensors $\boldsymbol{\mathcal{U}}$ and $\boldsymbol{\mathcal{V}}$

1: Obtain the capped inverse of $\boldsymbol{A}$ as in equation (47);
2: Construct selection matrices $\mathbf{J}_k$ as in equation (50);
3: **if** $LN < \sum_k M_k$ **then**
4: Construct set of shared subspaces $\mathcal{S}$ as described in equation (51) and allocate them according to greedy or fairness-aware strategies as in equations (52a) and (52b), respectively;
5: Augment selection matrices $\mathbf{J}_k$ as in equation (53);
6: **end if**
7: Calculate the TX powers $p_{k,q}$ as in equations (55) or (56), depending on the allocation strategy adopted (greedy or fairness-aware) and on the transmission mode (DL or UL);
8: Construct TX beamformers $\boldsymbol{V}_k$ as in equation (48);
9: Construct RX beamformers $\boldsymbol{U}_k$ as in equation (54);
10: Collect $\boldsymbol{V}_k$ into $\boldsymbol{\mathcal{V}}$ as in equation (11b), and $\boldsymbol{U}_k$ into $\boldsymbol{\mathcal{U}}$ as in equation (11c), respectively.

In the UL case, we obtain straightforwardly

$$\boldsymbol{U}_k^{\mathrm{u}} = \mathbf{J}_k^{\mathrm{T}} \boldsymbol{A}^{\dagger}. \tag{54b}$$

Finally, to complete the joint TX/RX BF scheme, the transmit powers allocated to each stream of each user under the greedy and fairness-aware strategies are respectively set to

$$p_{k,q} = \sqrt{P \frac{\left\| \mathbf{C}_k \cdot \langle \mathbf{J}_k \rangle_q \right\|_{\mathrm{F}}^2}{\sum_{k'} \| \mathbf{C}_{k'} \cdot \mathbf{J}_{k'} \|_{\mathrm{F}}^2}}, \tag{55a}$$

$$p_{k,q} = \sqrt{P \frac{\left\| \mathbf{C}_k \cdot \langle \mathbf{J}_k \rangle_q \right\|_{\mathrm{F}}^2}{\sum_{k'} \frac{\| \mathbf{C}_k \cdot \mathbf{J}_k \|_{\mathrm{F}}^4}{\| \mathbf{C}_{k'} \cdot \mathbf{J}_{k'} \|_{\mathrm{F}}^2}}}. \tag{55b}$$

For the UL case, we have

$$p_{k,q} = \sqrt{P_k \frac{\left\| \mathbf{C}_k \cdot \langle \mathbf{J}_k \rangle_q \right\|_{\mathrm{F}}^2}{\| \mathbf{C}_k \cdot \mathbf{J}_k \|_{\mathrm{F}}^2}}, \tag{56}$$

where we remark that in the UL case, a fairness-aware strategy is impractical due to the required assumption that the matrices $\mathbf{C}_{k'}$ and $\mathbf{J}_{k'}$, is known to all $k$-th UE, with $k' \neq k$.

For convenience, we summarize the proposed OEML-GSVD-based BF scheme for heterogeneous CF-mMIMO systems in Algorithm 3.

## IV. PERFORMANCE ASSESSMENT

In this section, we assess the performance of both the OEML-GSVD tensor decomposition and the corresponding heterogeneous TX/RX DL and UL BF schemes for CF-mMIMO proposed above and summarized in Algorithms 2 and 3, respectively. The assessment is conducted using Monte Carlo simulations both in terms of the convergence of the OEML-GSVD method itself, and in terms of the consequently attained gains in SE[4]in comparison with the state-of-the-art (SotA) MRC, MMSE, and FP beamformers. In addition, in order to highlight the gains obtained by the OEML-GSVD technique here described, the results are compared against those of beamformers obtained as described by Algorithm 3, but employing the ML-GSVD tensor decomposition scheme of [42] instead.

**TABLE 1.** Simulation parameters.

| Symbol | Meaning | Value |
|---|---|---|
| $L$ | Number of APs | Variable |
| $N$ | Number of AP's antenna | Variable |
| $K$ | Number of UEs | Variable |
| $M_k$ | Number of $k$-th UE's antenna | Variable |
| $h$ | Height of antennas | 10[m] [17] |
| $f_{\mathrm{c}}$ | Carrier frequency | 2[GHz] [17] |
| $B$ | Bandwidth | 20[MHz] [17] |
| $D$ | Length of a side of the square | 300[m] [61] |
| $\sigma^2$ | Receiver noise variance | -96[dBm] [17] |
| $P$ | Downlink TX power constraint | 45[dBm] |
| $P_k$ | Uplink TX power constraint | 20[dBm] |

Unless indicated otherwise in the caption or titles of corresponding figures, all simulations were carried out using the simulation parameters which are set according to recent related work, in particular [17], [61] and summarized in Table 1.

### A. COMPLEXITY ASSESSMENT

Let us start by assessing the computation complexity of the MMSE DL and UL BFs in the context of the article. The arithmetic complexity analysis in this section is based on the number of floating point operations required to execute a given BF algorithm.[5] First, notice that the most expensive operation in the MMSE scheme is the pseudo-inversion of the $LN \times LN$ matrix $\sum_{k'} \boldsymbol{H}_{k'}^{\mathrm{H}} \boldsymbol{H}_{k'} + \sigma_k^2 \mathbf{I}_{LN}$, which is required to design the DL TX BF matrix $\boldsymbol{V}_k^{\mathrm{d}}$ as per equation (14), or equivalently of the $LN \times LN$ matrix $\sum_{k'} \boldsymbol{H}_{k'}^{\mathrm{T}} \boldsymbol{H}_{k'}^{*} + \sigma_k^2 \mathbf{I}_{LN}$ of the UL RX BF matrix $\boldsymbol{U}_k^{\mathrm{u}}$, as per equation (14). That is, a MMSE BF requires a complexity of order $\mathcal{O}((LN)^3)$ both for the DL and UL. In addition, the MMSE also needs $K$ multiplications (*i.e.*, one per user) of the result of the latter inverse and the $LN \times M_k$ $k$-th channel matrix conjugate transpose $\boldsymbol{H}_k^{\mathrm{H}}$, in the case of equation (14), or the channel matrix $M_k \times LN$ $k$-th channel matrix conjugate, in the case of equation (14), with corresponding complexity of order $\mathcal{O}((LN)^2 \sum_{k=1}^{K} M_k)$. Furthermore, the computation of the terms $\sum_{k'} \boldsymbol{H}_{k'}^{\mathrm{H}} \boldsymbol{H}_{k'} + \sigma_k^2 \mathbf{I}_{LN}$ and $\sum_{k'} \boldsymbol{H}_{k'}^{\mathrm{T}} \boldsymbol{H}_{k'}^{*} + \sigma_k^2 \mathbf{I}_{LN}$ themselves requires the evaluation of the products $\boldsymbol{H}_{k'}^{\mathrm{H}} \boldsymbol{H}_{k'}$ and $\boldsymbol{H}_{k'}^{\mathrm{T}} \boldsymbol{H}_{k'}^{*}$, respectively, each of order $\mathcal{O}(M_k (LN)^2)$, for all $k' \in \{1, \ldots, K\}$, resulting in another computational cost contribution of $\mathcal{O}(K(LN)^2 \sum_{k=1}^{K} M_k)$ for all users. Consequently, the total computation complexity associated with DL and UL MMSE beamforming in CF-mMIMO systems is

$$\mathcal{O}\left( (LN)^3 + (LN)^2 (K+1) \sum_{k=1}^{K} M_k \right), \tag{57}$$

4. We remark that SE is the standard metric to evaluate the performance of CF-mMIMO systems as discussed in [16], [17].
5. The interested reader is kindly referred to related literature such as [62].

which readily reduces to

$$\mathcal{O}\left(\max\left\{(LN)^3, (LN)^2K\sum_{k=1}^{K}M_k\right\}\right), \tag{58}$$

where $\max\{\cdot\}$ returns the largest quantity among the inputs.

Next, we turn our attention to the computation complexity required by the FP-based BF design summarized in Algorithm 1. First of all, in order to design the FP based BF, the MMSE BF needs to be designed as the initial BF, which requires the computational complexity defined in equation (57). Since the required operations differ between DL and UL, we hereafter describe each complexity separately.

In DL, the FP-based BF requires updating $\mathbf{\Gamma}_k$ with inversion of the $M_k \times M_k$ matrix $\boldsymbol{E}_k^{\mathrm{d}}$ and several matrix-multiplication operations. Consequently, updating $\mathbf{\Gamma}_k$, $\forall k$ accounts for $\mathcal{O}(\sum_{k=1}^{K}\{2(LN)^2KM_k+LNKM_k^2+2M_k^3\})$ in total, followed by the auxiliary variable $\mathbf{\Psi}$ that contains inversion of the $M_k \times M_k$ matrix $(\sigma^2\mathbf{I}+\sum_{k\in\mathcal{K}}\boldsymbol{H}_k\boldsymbol{V}_k\boldsymbol{V}_k^{\mathrm{H}}\boldsymbol{H}_k^{\mathrm{H}})$ and several matrix-multiplication operations. In turn, in order to calculate $\mathbf{\Psi}_k$, $\forall k$, one needs $\mathcal{O}(\sum_{k=1}^{K}\{(2K+1)(LN)^2M_k+(K+1)LNM_k^2+M_k^3\})$. Denoting $\zeta$ as the number of iterations for bisection search to solve equation (24), the complexity for $\boldsymbol{V}_k\,\forall k$ can be estimated as $\mathcal{O}(\zeta((LN)^3+\sum_{k=1}^{K}(LN)^2(K+1)M_k+LN(3K+2)M_k^2))$. All in all, the total dominant computational complexity of the FP-based BF in DL is

$$\mathcal{O}\Bigg((1+\beta\zeta)(LN)^3+(LN)^2\{\beta(\zeta K+\zeta+4K+1)+(K+1)\}\sum_{k=1}^{K}M_k + LN\beta(3\zeta K+2\zeta+2K+1)\sum_{k=1}^{K}M_k^2+3\beta\sum_{k=1}^{K}M_k^3\Bigg), \tag{59}$$

where $\beta$ is the number of outer-loop iterations in Algorithm 1.

The latter expression can be conveniently written as

$$\mathcal{O}\left(\max\left\{T_1^{\mathrm{d}}, T_2^{\mathrm{d}}, T_3^{\mathrm{d}}, T_4^{\mathrm{d}}\right\}\right), \tag{60}$$

where

$$T_1^{\mathrm{d}} = \beta\zeta(LN)^3, \tag{61a}$$

$$T_2^{\mathrm{d}} = \beta\zeta(LN)^2K\sum_{k=1}^{K}M_k, \tag{61b}$$

$$T_3^{\mathrm{d}} = \beta\zeta LNK\sum_{k=1}^{K}M_k^2, \tag{61c}$$

$$T_4^{\mathrm{d}} = \beta\sum_{k=1}^{K}M_k^3. \tag{61d}$$

As for UL, the associated complexity is the same as that of DL except for updates of $\boldsymbol{U}_k$ for all $k$, the most expensive operation of which is the inversion of an $LNM_k \times LNM_k$ matrix and the Kronecker product of $LN \times LN$ and $M_k \times M_k$ matrices, amounting to $\mathcal{O}(\zeta\sum_{k=1}^{K}\{(LNM_k)^3+(LN)^2M_k(1+2M_k)+LNM_k^2+3M_k^3\})$, such that the total dominant complexity for the FP-based BF design for UL is given by

$$\mathcal{O}\Bigg((LN)^3\left(1+\beta\zeta\sum_{k=1}^{K}M_k^3\right) + (LN)^2\sum_{k=1}^{K}M_k\{\beta(\zeta K+2\zeta M_k+4K+1)+(K+1)\} + LN\beta(\zeta+2K+1)\sum_{k=1}^{K}M_k^2+3(\zeta+1)\sum_{k=1}^{K}M_k^3\Bigg), \tag{62}$$

which again can be rewritten as

$$\mathcal{O}\left(\max\left\{T_1^{\mathrm{u}}, T_2^{\mathrm{u}}, T_3^{\mathrm{u}}, T_4^{\mathrm{u}}\right\}\right), \tag{63}$$

with

$$T_1^{\mathrm{u}} = \beta\zeta(LN)^3\sum_{k=1}^{K}M_k^3, \tag{64a}$$

$$T_2^{\mathrm{u}} = \beta\zeta(LN)^2\sum_{k=1}^{K}M_k(K+M_k), \tag{64b}$$

$$T_3^{\mathrm{u}} = LN\beta(\zeta+K)\sum_{k=1}^{K}M_k^2, \tag{64c}$$

$$T_4^{\mathrm{u}} = \beta\zeta\sum_{k=1}^{K}M_k^3. \tag{64d}$$

Finally, let us address the complexity of the proposed OEML-GSVD-based DL and UL BF scheme. To that end, we must take into account both the complexities of the OEML-GSVD tensor decomposition described in Algorithm 2, as well as the design of TX and RX DL and UL beamforming matrices $\boldsymbol{V}_k^{\mathrm{d}}$, $\boldsymbol{U}_k^{\mathrm{d}}$, $\boldsymbol{V}_k^{\mathrm{u}}$ and $\boldsymbol{U}_k^{\mathrm{u}}$, as described in Algorithm 3.

One of the most expensive operations in Algorithm 2 is the update of $\boldsymbol{B}_k$, as per equation (35), which requires both the inversion and square-rooting $(\cdot)^{-\frac{1}{2}}$, whose cost if implemented via SVD is of order $\mathcal{O}((LN)^3+(LN)^2)$ per UE, and the various matrix multiplications, whose complexities add up to $\mathcal{O}((LN)^3+M_k(LN)^2)$ per UE. The total cost of updating $\boldsymbol{B}_k$ is therefore $\mathcal{O}(K(LN)^3+(LN)^2(K+\sum_{k=1}^{K}M_k))$.

In turn, the matrix multiplications required to update the matrices $\mathbf{C}$ and $\boldsymbol{A}$, as per equations (37) and (45), also contribute with additional computational costs. In particular, equation (37) requires the multiplication of $K \times (LN)^2$, $(LN)^2 \times (LN)$, and $LN \times LN$ matrices, at cost $\mathcal{O}(K(LN)^3+K(LN)^2)$, while equation (45) involves the multiplication of $LN \times LNK$ and $LNK \times LN$ matrices, at cost $\mathcal{O}(K(LN)^3)$. Collecting all these contributions, the total computation complexity of Algorithm 2 is of order

$$\mathcal{O}\left(\alpha K(LN)^3+\alpha(LN)^2\left(K+\sum_{k=1}^{K}M_k\right)\right), \tag{65}$$

where $\alpha$ is the number of outer-loop iterations in Algorithm 2.

Next we turn our attention to the computational complexity of the DL and UL BF schemes of Algorithm 3, given the decomposed tensor $\boldsymbol{\mathcal{H}}$ in the form of the tensor $\boldsymbol{\mathcal{B}}$ and the matrices $\mathbf{C}$ and $\boldsymbol{A}$ obtained from Algorithm 2.

There the first major cost is the computation of the capped pseudo-inverse of the matrix $\boldsymbol{A} \in \mathbb{C}^{LN\times LN}$ described by equation (47), which has complexity of order $\mathcal{O}((LN)^3 + (LN)^2)$ due to the required SVD of the matrix $\boldsymbol{A}$.

Additional major costs are the matrix multiplications required for the computation of the beamforming matrices themselves, as per equations (48) and (54). In particular, in the DL, the TX BF matrix $\boldsymbol{V}_k^{\mathrm{d}}$ is constructed row-by-row as in equation (48a), at the cost $\mathcal{O}(Q_k(LN)^2)$ per user, while the RX BF matrix $\boldsymbol{U}_k^{\mathrm{d}}$ is obtained as in equation (54a), with cost of order $\mathcal{O}(LNM_kQ_k)$ per user. Similar costs are required to evaluate equations (48b) and (54b) in order to obtain the UL TX and RX BF matrices $\boldsymbol{V}_k^{\mathrm{u}}$ and $\boldsymbol{U}_k^{\mathrm{u}}$, respectively. All in all, the total complexity of Algorithm 3 is of order

$$\mathcal{O}\left((LN)^3 + (LN)^2\sum_{k=1}^{K} Q_k + LN\sum_{k=1}^{K} M_kQ_k\right), \tag{66}$$

such that altogether, the computational complexity order of the proposed OEML-GSVD-based DL and UL BF schemes, including both Algorithms 2 and 3, is

$$\mathcal{O}\Bigg((\alpha K+1)(LN)^3 + (LN)^2\left(\alpha K + \alpha\sum_{k=1}^{K} M_k + Q_k\right) + LN\sum_{k=1}^{K} M_kQ_k\Bigg), \tag{67}$$

which can be simplified by specifying the dominant term as

$$\mathcal{O}\big(\max\{T_1^{\mathrm{pro}}, T_2^{\mathrm{pro}}, T_3^{\mathrm{pro}}\}\big), \tag{68}$$

with

$$T_1^{\mathrm{pro}} = \alpha K(LN)^3, \tag{69a}$$

$$T_2^{\mathrm{pro}} = \alpha(LN)^2(K + \sum_{k=1}^{K} M_k), \tag{69b}$$

$$T_3^{\mathrm{pro}} = LN\sum_{k=1}^{K} M_kQ_k. \tag{69c}$$

A very interesting insight can be concluded from the coarse complexity analysis made above. In particular, consider a fully-loaded system in which the total number of user antennas is equal to the number of antennas of the collection of APs, *i.e.*, $\sum_{k=1}^{K} M_k = LN$, which can therefore be seen as an upper bound in terms of computational complexity as $\sum_{k=1}^{K} M_k < LN$ is assumed. Then, the analysis indicates that the conventional MMSE BF scheme in a CF-mMIMO setup has complexity of order

$$\mathcal{O}\Big((LN)^3 + (LN)^2(K+1)LN\Big) = \mathcal{O}\Big(K(LN)^3\Big), \tag{70}$$

which implicates that the worst case scenario for a CF-mMIMO employing MMSE beamforming is the fully-loaded full-capacity scenario, when the system serves a number $K = LN$ of single-antenna users, with complexity

$$\mathcal{O}\Big((LN)^4\Big). \tag{71}$$

In turn, with the proposed OEML-GSVD-based beamforming scheme, fully loaded conditions imply, besides $\sum_{k=1}^{K} M_k = LN$, also the equality $M_k = Q_k$ for all $k$, which yields complexity

$$\begin{aligned}\mathcal{O}&\left((\alpha K+1)(LN)^3 + \alpha K(LN)^2 + LN\sum_{k=1}^{K} M_k^2\right)\\ &\le \mathcal{O}\Big((\alpha K+2)(LN)^3 + \alpha K(LN)^2\Big),\end{aligned} \tag{72}$$

where the latter upper-bound follows from the Cauchy-Schwartz inequality.

Comparing equations (70) and (72), we can conclude that the complexity of the proposed OEML-GSVD-based beamforming scheme for CF-mMIMO systems under fully loaded conditions is of the same order of magnitude (*i.e.*, cubic on $LN$), as that of the SotA alternative based on MMSE.

Better still, in the fully loaded full-capacity case when the equality $M_k = Q_k = 1$ also holds, equation (72) reduces to

$$\mathcal{O}\Big(\alpha(LN)^4\Big). \tag{73}$$

Therefore, when the number of iterations $\alpha$ is small enough, the complexity of the OEML-GSVD is similar to that of the MMSE beamforming approach in fully loaded CF-mMIMO under full user capacity conditions, as given in equation (71).

Finally, recall that the FP-based approach is of a significantly larger complexity order than the OEML-GSVD, as shown in (63). As shall be shown in Section IV-C, despite having MMSE-like computational complexity, the proposed OEML-GSVD-based beamforming scheme yields significant spectral efficiency gains over the MMSE approach, which qualifies the relevance of our contribution.

### B. CONVERGENCE

In this subsection, we evaluate the convergence of our proposed OEML-GSVD. The state-of-the-art ML-GSVD algorithm [42] is based on a direct fitting (DF) algorithm whose convergence is guaranteed [39]. Although the proposed OEML-GSVD algorithm is also based on the DF algorithm, a nonlinear flipping operation is incorporated so as to enforce the orthogonality in Algorithm 2, which imposes a challenge in theoretically guaranteeing convergence. Thus, the convergencce of the proposed decompostion algorithm is evaluated empirically for different parameter setups, in which we evaluate the convergence not only for the underloaded scenarios $LN > \sum_k M_k$ but also for fully- and over-loaded conditions for the sake of completeness. In order to evaluate the convergence of the algorithm, let us introduce the mean aggregate normalized fitting error, which

captures the overall average error of a tensor decomposition and is given by

$$E^{(i)} \triangleq \mathbb{E}\left[\frac{\sum_k \left\|\boldsymbol{W}_k^{(i)}\right\|_{\mathrm{F}}^2}{\sum_k \|\boldsymbol{H}_k\|_{\mathrm{F}}^2}\right], \tag{74}$$

where $\boldsymbol{W}_k^{(i)}$ is the fitting error of the $k$-th slice of the tensor $\boldsymbol{\mathcal{H}}$ at the $i$-th iteration of the decomposition, and the expectation $\mathbb{E}[\cdot]$ is taken over multiple realizations of $\boldsymbol{\mathcal{H}}$.

Using the latter metric, the convergence of the proposed OEML-GSVD in underloaded, fully loaded, and overloaded conditions are depicted in Figure 4. For the sake of comparison, plots for the ML-GSVD algorithm of [42] are also shown. It is found that OEML-GSVD outperforms the preceding ML-GSVD in terms of accuracy by a factor of 10, both in under- and fully-loaded conditions, without a significant penalty in terms of the required number of iterations until convergence.

This gain is attributed to the orthogonality-enforcing operations represented by equations (39) to (44), which in under- and fully-loaded conditions lead to binary and maximally sparse matrices $\mathbf{C}$. In the underloaded case in particular, when $LN > \sum_k M_k$, the matrix $\mathbf{C}$ outputted by the OEML-GSVD algorithm contains exactly $LN - \sum_k M_k$ all-zero columns, in contrast to the ML-GSVD method where such a structure of the matrix $\mathbf{C}$ is not allowed, even in the underloaded set up.

On the other hand, it is also seen that the orthogonality-enforcing operations cause small fluctuations in normalized error $E^{(i)}$ in OEML-GSVD, which result form equations (41) and in particular (44), where a subset of free subspaces are randomly allocated to different slices of the tensor $\boldsymbol{\mathcal{H}}$ in order to fully exploit available spatial resources.

In fact, this crucial distinction between the OEML-GSVD and the ML-GSVD methods diminishes in the overloaded case, which is why the OEML-GSVD is found to outperform the ML-GSVD only slightly in the overloaded case, with the advantage of the former over the latter more pronounced in the fully-loaded case and more so in the underloaded case.

All in all, the results motivates the claim that the OEML-GSVD tensor decomposition is generally superior to ML-GSVD, yielding a more accurate representation of the tensor $\boldsymbol{\mathcal{H}}$ in subspaces with as little overlap among its slices as possible, in comparison to current literature.

### C. SINGLE-ANTENNA VS MULTI-ANTENNA USERS

Our first comparisons aim at avoiding any possible misunderstanding that a system serving UEs equipped with multiple antennas could be optimized in a manner equivalent to a system with a larger number of single-antenna UEs.

In particular, we highlight that such equivalence only holds in the ideal case of fully-uncorrelated channels per antenna, while it is considered that spatial correlation may occur, as modeled by the matrix $\boldsymbol{R}_{\ell,k} \in \mathbb{C}^{M_k \times M_k}$ in equation (1).

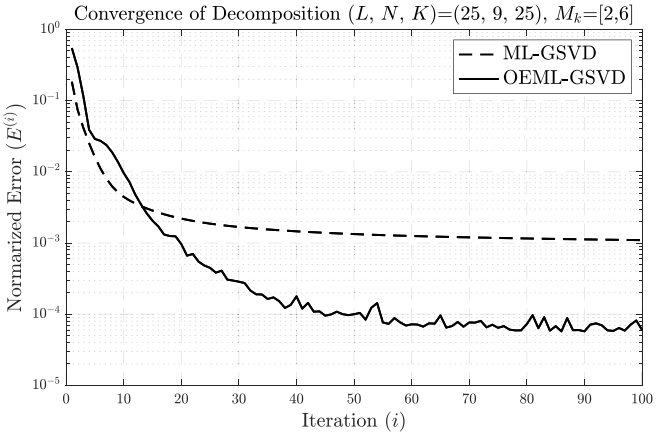


(a) Underloaded

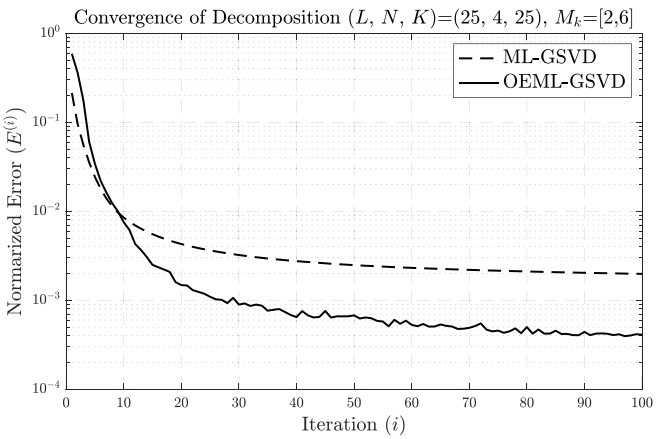


(b) Fully loaded

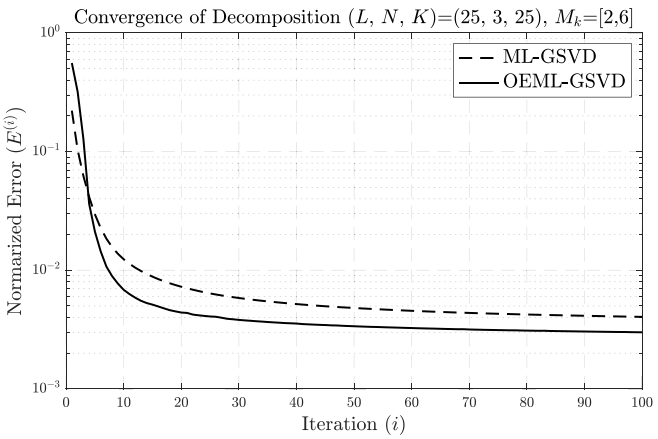


(c) Overloaded

**FIGURE 4.** Convergence behaviors of OEML-GSVD and ML-GSVD methods.

Figures 5 and 6 compare the cumulative distribution function (CDF) of the total SE $\eta$ in DL and UL scenarios, respectively, with CDFs obtained from multiple UE positions and channel realizations. In the figures, we compare the performance of the OEML-GSVD-based joint TX/RX DL and UL BF schemes against results obtained with the MRC, MMSE, and FP-based beamformers, as well as with

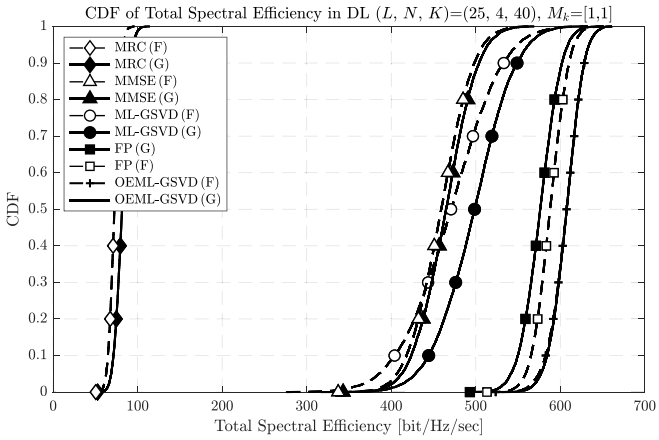


(a) Scenario with single-antenna UEs.

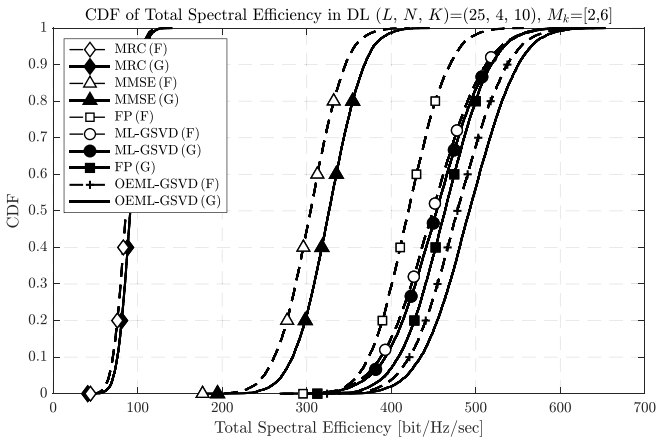


(b) Scenario with multi-antenna UEs.

**FIGURE 5.** Total SE performances of CF-mMIMO systems with different user/antenna configurations, in DL.

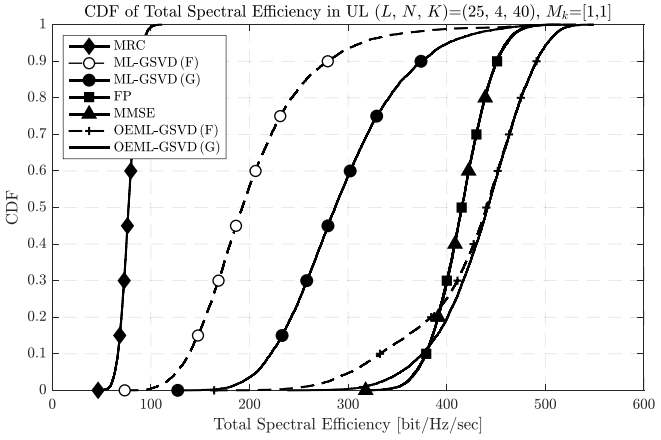


(a) Scenario with single-antenna UEs.

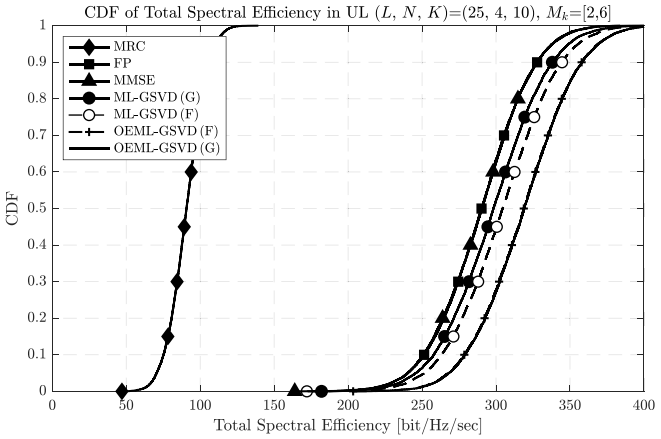


(b) Scenario with multi-antenna UEs.

**FIGURE 6.** Total SE performances of CF-mMIMO systems with different user/antenna configurations, in UL.

the preceding ML-GSVD scheme. As for the power allocation schemes employed, we offer results for all these methods both under the greedy (G) and the fairness-aware (F) resource allocation strategies described in equations (52a) and (52b), respectively.

The figures clearly illustrate the fact that the SEs in DL and UL differ under the presence of spatial correlation, as expected. Interestingly, it is in fact found from this comparison that the proposed OEML-GSVD-based CF-mMIMO-BF scheme not only outperforms all other alternatives in both DL and UL, but also achieves its own best performance in the scenario where all UEs are single-antenna devices due to the fact that the single-antenna scenario results in additional spatial DoF in comparison with multiple-antennas scenario thanks to the absence of spatial correlation.

The results indicate that the orthogonality between UEs enforced by the flipping operation in the proposed method indeed yields performance improvement over the preceding ML-GSVD scheme by better suppressing inter-user interference. It is worth emphasizing that this enforced orthogonality also results in better decomposition accuracy as already shown in Figure 4. In turn, in the comparison between OEML-GSVD and conventional BF designs such as MRC, MMSE, and FP-based BF, the gain is brought by the joint TX and RX BF capability of the proposed method, which comes with significantly lower communication overhead and computational complexity as shown in the complexity analysis of the previous subsection.

Notice that we consider BF capability only at APs for the conventional BF designs, since to the best of our knowledge, there is no existing mechanism to jointly design TX and RX BFs and power allocation for user-heterogeneous CF-mMIMO systems. Although the FP-based BF design can be extended to a joint TX/RX BF design in an alternative optimization manner, in which TX and RX BFs are iteratively updated, this comes with additional complexity costs and higher overhead to unicast the BF matrix to each UE, which jointly limit the scalability of the CF-mMIMO system.

### *D. SE ANALYSIS: MULTI-ANTENNAS UEs*

Having clarified the fact that the SE performance indeed differs between single and multiple antennas UEs, which might be obvious to some readers but which is worthy to avoid

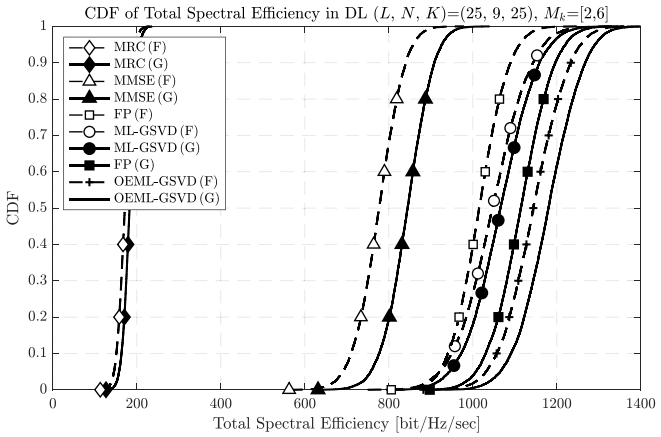


(a) Total SE

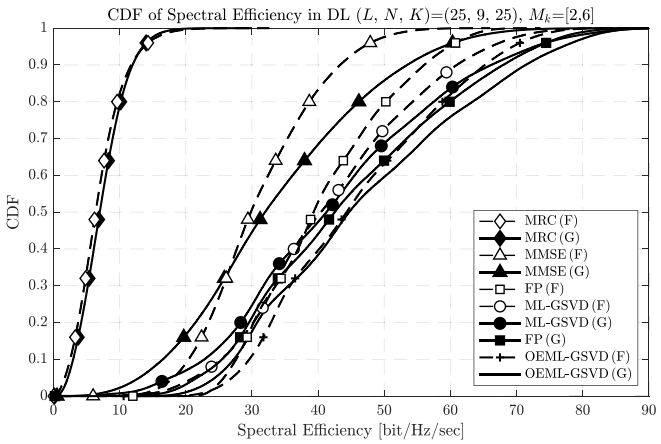


(b) SE of each UE

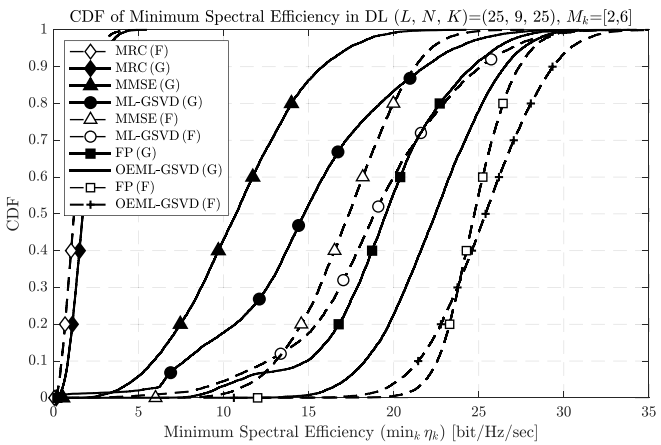


(c) Minimum SE

**FIGURE 7.** **Distribution of DL SE achieved with conventional and proposed OEML-GSVD beamformers.**

any doubts, we further offer different CDF comparisons in this section to seek deeper insight on the advantage of the proposed OEML-GSVD approach. In Figure 7 and 8, a set of CDFs of the SE performance of all the BF methods in DL and UL is respectively shown to analyse the SE from different aspects. To elaborate, Figure 7(a) and 8(a) corresponds to the total SE performance in DL and UL, respectively, while Figure 7(b) and 8(b) respectively shows the CDF of the DL and UL SE performance obtained at each UE. In turn, the CDF of the minimum SE performance among all the UEs for a given channel realization is respectively shown for DL and UL cases in Figure 7(c) and 8(c).

We remark that in the DL case depicted in Figure 7, the greedy and fairness-aware strategies of the MRC, MMSE and FP-based methods reduce to mere greedy and fairness-aware power allocations in accordance with equations (15a) and (15b), due to limitations of these schemes. In contrast, in the proposed OEML-GSVD-based BF scheme, these strategies include the allocation of orthogonal subspaces as described in equations (52a) and (52b), as well as the corresponding power allocations of equations (55a) and (55b). It is found, non-surprisingly, that the proposed joint TX/RX BF scheme based on the OEML-GSVD tensor decomposition here introduced significantly outperforms the conventional MRC, MMSE, and FP, as well as the method based on the ML-GSVD tensor decomposition of [42]. The OEML-GSVD-based BF design can outperform the FP-based BF due to the fact that the proposed method exclusively allocates spatial resources to UEs similarly to orthogonal multiple access (OMA) systems, nearly eliminating inter-user interference if spatial resources are sufficient.

Since CF-mMIMO systems are originally and generally referred to as a distributed MIMO setup with the number of APs greater than the number of UEs [17], [19], the proposed method is especially suited for CF-mMIMO systems. In terms of user-fairness, it can also be seen from Figure 7(c) that the fairness-aware (F) resource allocation strategy results in significant fairness performance improvements over the greedy (G) counterpart.

Comparing the proposed method with the MRC and MMSE, it is noticeable that fairness-aware OEML-GSVD greatly outperforms the classic alternatives even in full greedy mode. It can also be seen, furthermore, that the gap between the results obtained with the proposed scheme with greedy and fairness-aware allocations is much wider than those observed with the MRC and MMSE beamformers, which highlights the role of the improvements achieved thanks to the new OEML-GSVD.

Similar results can be seen also from Figure 8 in the UL case, where the proposed algorithm demonstrates superior performance against the other methods from three distinct SE aspects. Besides that, we also emphasize that the curves corresponding to the ML-GSVD method included in Figure 8 are also original, since the application of the tensor decomposition to the UL case was not considered in the original article [42].

All in all, the set of comparisons above demonstrates that the proposed OEML-GSVD beamformer is effective in mitigating inter-user interference, allocating the available resources to users more efficiently than existing approaches.

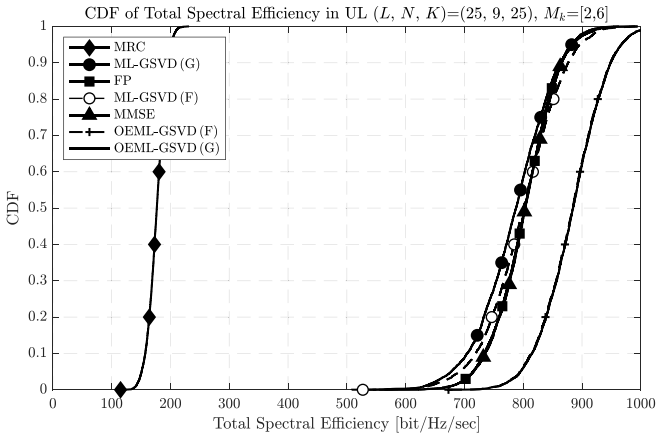


(a) Total SE

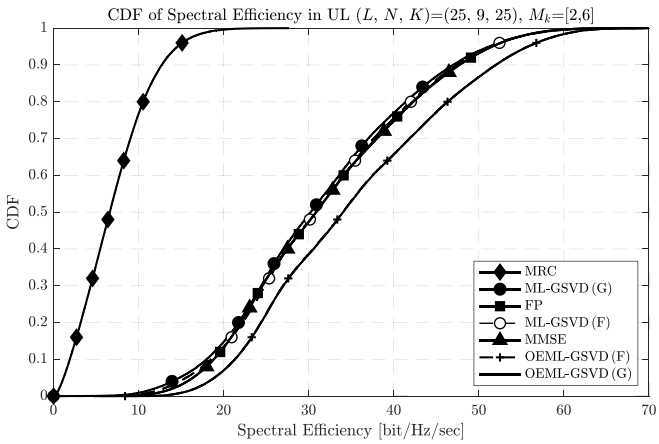


(b) SE of each UE

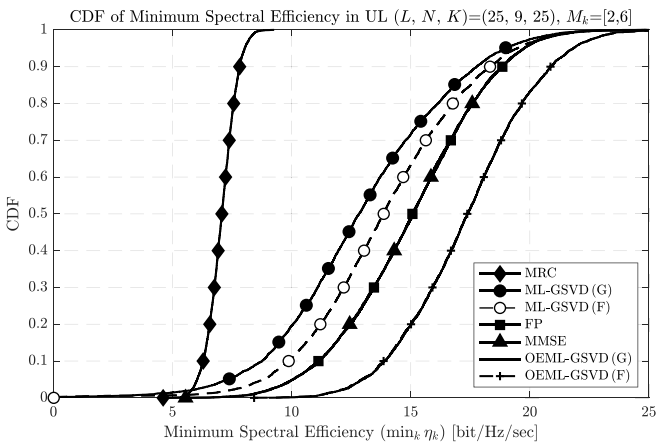


(c) Minimum SE

**FIGURE 8.** **Distribution of UL SE achieved with conventional and proposed OEML-GSVD beamformers.**

## V. CONCLUSION

In this article, we proposed an improved tensor-decomposition method enforcing exclusive use of available spatial resources, dubbed the orthogonality-enforcing ML-GSVD (OEML-GSVD), paving the way towards a new framework for the design of effective DL and UL BF schemes for CF-mMIMO. Thanks to this improved tensor decomposition, the multiple streams sent to and received from the users of a CF-mMIMO system can be separated into dedicated private subspaces without inter-user interference, selected according to a mapping that leads to better spectral efficiency with or without fairness, and allocated to the various users with corresponding optimized powers, regardless of the differences in the number of antennas among them.

Numerical results demonstrate that the proposed OEML-GSVD method outperforms its predecessor ML-GSVD in accuracy without sacrificing convergence speed, and that as a result the corresponding joint TX/RX DL and UL beamformers yield superior performance compared both to classical state-of-the-art methods such as MMSE, MRC, and FP-based approaches, as well as similar methods based on the ML-GSVD tensor decomposition. The complexity analysis of the proposed method compared to the conventional MMSE alternative indicates that these gains also are reaped without a significant increase in computational complexity order over that classic approach.

As a follow up work, it would be relevant to further extend the proposed BF design to incorporate practical aspects such as scalability and/or CSI imperfection. A possible extension to improve scalability is to combine user-centric clustering mechanisms with the tensor-based BF design, aiming at reducing the CSI collection overhead at the CPU the centrality of the operation. The resulting system would likely not exhibit the same performance of those shown here, but such an extension might offer an excellent compromise between the SE performance and scalability. Another possible extension is to revise the system design so as to improve robustness against CSI imperfection. To that end, assuming that CSI imperfection can be modeled as an additive error, robustness can be obtained by observing that such CSI imperfection/error can be incorporated into the fitting error $\boldsymbol{W}_k^{(i)}$ of equation (31). Then, if statistical knowledge on the CSI imperfection is available, the optimization of $\boldsymbol{B}_k$ shown in equation (33) can be modified accordingly, for instance, by replacing the objective $\mathrm{Tr}\big(\boldsymbol{W}_k\boldsymbol{W}_k^{\mathrm{H}}\big)$ with the mean square error $\mathbb{E}\big[\mathrm{Tr}\big(\boldsymbol{W}_k\boldsymbol{W}_k^{\mathrm{H}}\big)\big]$.

Finally, in order to accommodate for further robustness such as cases in which channel estimation is affected by pilot contamination, a joint CSI estimation and beamforming design would be required. To that end, however, the authors consider that smart way to go would be to integrate the channel estimation and beamforming design, leading to a joint channel estimation and beamforming approach. Inspiring examples in that direction are the joint channel estimation design proposed for massive MIMO systems in [63], and the method for CF-mMIMO systems with single-antenna UEs proposed in [30].

## ACKNOWLEDGEMENT

The authors would like to thank Ms. L. Khamidullina for her helpful comments and reference code for reproduction of the ML-GSVD.

## REFERENCES


[1] W. Ejaz, A. Anpalagan, M. A. Imran, M. Jo, M. Naeem, S. B. Qaisar, and W. Wang, "Internet of Things (IoT) in 5G wireless communications," *IEEE Access*, vol. 4, pp. 10 310–10 314, 2016.

[2] S. A. Ashraf, R. Blasco, H. Do, G. Fodor, C. Zhang, and W. Sun, "Supporting vehicle-to-everything services by 5G new radio release-16 systems," *IEEE Communications Standards Magazine*, vol. 4, no. 1, pp. 26–32, 2020.

[3] W. Saad, M. Bennis, and M. Chen, "A vision of 6G wireless systems: Applications, trends, technologies, and open research problems," *IEEE Network*, vol. 34, no. 3, pp. 134–142, 2020.

[4] S. Rangan, T. S. Rappaport, and E. Erkip, "Millimeter-wave cellular wireless networks: Potentials and challenges," *Proc. IEEE*, vol. 102, no. 3, pp. 366–385, Mar. 2014.

[5] J. Choi, V. Va, N. Gonzalez-Prelcic, R. Daniels, C. R. Bhat, and R. W. Heath, "Millimeter-wave vehicular communication to support massive automotive sensing," *IEEE Communications Magazine*, vol. 54, no. 12, pp. 160–167, 2016.

[6] H. Iimori, G. T. F. de Abreu, O. Taghizadeh, R.-A. Stoica, T. Hara, and K. Ishibashi, "A stochastic gradient descent approach for hybrid mmwave beamforming with blockage and CSI-error robustness," *IEEE Access*, vol. 9, pp. 74 471–74 487, May 2021.

[7] A. Ghods, S. Severi, and G. Abreu, "Localization in V2X communication networks," in *2016 IEEE Intelligent Vehicles Symposium*, 2016, pp. 5–9.

[8] H. Kim, K. Granström, L. Gao, G. Battistelli, S. Kim, and H. Wymeersch, "5G mmWave cooperative positioning and mapping using multi-model PHD filter and map fusion," *IEEE Transactions on Wireless Communications*, vol. 19, no. 6, pp. 3782–3795, 2020.

[9] S. Yang and L. Hanzo, "Fifty years of MIMO detection: The road to large-scale MIMOs," *IEEE Commun. Surveys Tut.*, vol. 17, no. 4, pp. 1941–1988, Fourthquarter 2015.

[10] L. H. Shen, K. T. Feng, and L. Hanzo, "Coordinated multiple access point multiuser beamforming training protocol for millimeter wave WLANs," *IEEE Transactions on Vehicular Technology*, vol. 69, no. 11, pp. 13 875–13 889, 2020.

[11] H. Iimori, G. T. F. de Abreu, O. Taghizadeh, R.-A. Stoica, T. Hara, and K. Ishibashi, "Stochastic learning robust beamforming for millimeter-wave systems with path blockage," *IEEE Wireless Commun. Lett.*, vol. 9, no. 9, pp. 1557–1561, Sept. 2020.

[12] T. L. Marzetta, "Noncooperative cellular wireless with unlimited numbers of base station antennas," *IEEE Trans. Wireless Commun.*, vol. 9, no. 11, pp. 3590–3600, 2010.

[13] F. Rusek, D. Persson, B. K. Lau, E. G. Larsson, T. L. Marzetta, O. Edfors, and F. Tufvesson, "Scaling up MIMO: Opportunities and challenges with very large arrays," *IEEE Signal Process. Mag.*, vol. 30, no. 1, pp. 40–60, 2013.

[14] R. Taniguchi, K. Nishimori, R. Kataoka, K. Kameyama, K. Kitao, N. Tran, and T. Imai, "Evaluation of massive MIMO considering real propagation characteristics in the 20-Ghz band," *IEEE Trans. Antennas Propag.*, vol. 65, no. 12, pp. 6703–6711, 2017.

[15] L. Sanguinetti, E. Bjornson, and J. Hoydis, "Fundamental asymptotic behavior of (two-user) distributed massive MIMO," in *Proc. IEEE GLOBECOM*, Dec 2018, pp. 1–6.

[16] E. Björnson and L. Sanguinetti, "Scalable cell-free massive MIMO systems," *IEEE Trans. Commun.*, vol. 68, no. 7, pp. 4247–4261, 2020.

[17] ——, "Making cell-free massive MIMO competitive with MMSE processing and centralized implementation," *IEEE Trans. Wireless Commun.*, vol. 19, no. 1, pp. 77–90, 2020.

[18] C. Liu, W. Feng, Y. Chen, C. Wang, and N. Ge, "Cell-free satellite-UAV networks for 6G wide-area Internet of Things," *IEEE Journal on Selected Areas in Communications*, pp. 1–1, 2020.

[19] H. Q. Ngo, A. Ashikhmin, H. Yang, E. G. Larsson, and T. L. Marzetta, "Cell-free massive MIMO versus small cells," *IEEE Trans. Wireless Commun.*, vol. 16, no. 3, pp. 1834–1850, 2017.

[20] H. Yang and T. L. Marzetta, "Energy efficiency of massive MIMO: Cell-free vs. cellular," in *2018 IEEE 87th Vehicular Technology Conference (VTC Spring)*, 2018, pp. 1–5.

[21] E. Nayebi, A. Ashikhmin, T. L. Marzetta, H. Yang, and B. D. Rao, "Precoding and power optimization in cell-free massive MIMO systems," *IEEE Trans. Wireless Commun.*, vol. 16, no. 7, pp. 4445–4459, Jul. 2017.

[22] T. C. Mai, H. Q. Ngo, M. Egan, and T. Q. Duong, "Pilot power control for cell-free massive MIMO," *IEEE Trans. Veh. Technol.*, vol. 67, no. 11, pp. 11 264–11 268, 2018.

[23] H. Liu, J. Zhang, S. Jin, and B. Ai, "Graph coloring based pilot assignment for cell-free massive MIMO systems," *IEEE Trans. Veh. Technol.*, vol. 69, no. 8, pp. 9180–9184, 2020.

[24] H. Iimori, T. Takahashi, K. Ishibashi, G. T. F. de Abreu, and W. Yu, "Grant-free access via bilinear inference for cell-free MIMO with low-coherence pilots," *IEEE Trans. Wireless Commun.*, vol. 20, no. 11, pp. 7694–7710, Nov. 2021.

[25] Y. Jin, J. Zhang, S. Jin, and B. Ai, "Channel estimation for cell-free mmWave massive MIMO through deep learning," *IEEE Trans. Veh. Technol.*, vol. 68, no. 10, pp. 10 325–10 329, 2019.

[26] S. Buzzi and C. D'Andrea, "Cell-free massive MIMO: User-centric approach," *IEEE Wireless Commun. Letters*, vol. 6, no. 6, pp. 706–709, Dec. 2017.

[27] G. Femenias, N. Lassoued, and F. Riera-Palou, "Access point switch on/off strategies for green cell-free massive MIMO networking," *IEEE Access*, vol. 8, pp. 21 788–21 803, 2020.

[28] K. Ando, H. Iimori, T. Takahashi, K. Ishibashi, and G. T. F. de Abreu, "Uplink signal detection for scalable cell-free massive MIMO systems with robustness to rate-limited fronthaul," *IEEE Access*, vol. 9, pp. 102 770–102 782, Jul. 2021.

[29] Y. Zhang, H. Cao, M. Zhou, and L. Yang, "Cell-free massive MIMO: Zero forcing and conjugate beamforming receivers," *Journal of Commun. and Networks*, vol. 21, no. 6, pp. 529–538, 2019.

[30] A. Zhou, J. Wu, E. G. Larsson, and P. Fan, "Max-min optimal beamforming for cell-free massive MIMO," *IEEE Commun. Letters*, vol. 24, no. 10, pp. 2344–2348, 2020.

[31] T. C. Mai, H. Q. Ngo, and T. Q. Duong, "Uplink spectral efficiency of cell-free massive MIMO with multi-antenna users," in *Proc SigTelCom, Hanoi, Vietnam,*, 2019, pp. 126–129.

[32] ——, "Downlink spectral efficiency of cell-free massive MIMO systems with multi-antenna users," *IEEE Trans. Commun.*, vol. 68, no. 8, pp. 4803–4815, 2020.

[33] A. J. Goldsmith and P. P. Varaiya, "Capacity of fading channels with channel side information," *IEEE Trans. Inform. Theory*, vol. 43, no. 6, pp. 1986–1992, 1997.

[34] C. F. V. Loan, "Generalizing the singular value decomposition," *SIAM Journal on Numerical Analysis*, vol. 13, no. 1, pp. 76–83, 1976. [Online]. Available: http://www.jstor.org/stable/2156468

[35] D. Senaratne and C. Tellambura, "GSVD beamforming for two-user MIMO downlink channel," *IEEE Trans. Veh. Technol.*, vol. 62, no. 6, pp. 2596–2606, 2013.

[36] R. A. Horn and C. R. Johnson, *Matrix Analysis, Second Edition*. Cambridge University Press, 2012.

[37] P. Comon, "Tensors : A brief introduction," *IEEE Signal Process. Mag.*, vol. 31, no. 3, pp. 44–53, 2014.

[38] A. Cichocki, D. Mandic, L. De Lathauwer, G. Zhou, Q. Zhao, C. Caiafa, and H. A. PHAN, "Tensor decompositions for signal processing applications: From two-way to multiway component analysis," *IEEE Signal Process. Mag.*, vol. 32, no. 2, pp. 145–163, 2015.

[39] H. Kiers, J. Berge, and R. Bro, "PARAFAC2—Part I. A direct fitting algorithm for the PARAFAC2 model," *Journal of Chemometrics*, vol. 13, pp. 275–294, 05 1999.

[40] K. Naskovska, M. Haardt, and A. L. F. de Almeida, "Generalized tensor contractions for an improved receiver design in MIMO-OFDM systems," in *Proc. IEEE ICASSP , Calgary, AB*, 2018, pp. 3186–3190.

[41] Y. Cheng and M. Haardt, "Enhanced direct fitting algorithms for PARAFAC2 with algebraic ingredients," *IEEE Signal Process. Letters*, vol. 26, no. 4, pp. 533–537, 2019.

[42] L. Khamidullina, A. L. F. de Almeida, and M. Haardt, "Multilinear generalized singular value decomposition (ml-gsvd) with application to coordinated beamforming in multi-user MIMO systems," in *Proc. IEEE ICASSP , Barcelona, Spain*, 2020, pp. 4587–4591.

[43] S. P. Ponnapalli, M. A. Saunders, C. F. V. Loan, and O. Alter, "A higher-order generalized singular value decomposition for comparison of global mRNA expression from multiple organisms," *PLoS ONE*, vol. 6, no. 12, 2011.

[44] X. Xiao, A. Moreno-Moral, M. Rotival, L. Bottolo, and E. Petretto, "Multi-tissue analysis of co-expression networks by higher-order generalized singular value decomposition identifies functionally coherent transcriptional modules," *PLoS ONE*, vol. 10, no. 1, 2014.

[45] N. J. Mayhall, "Using higher-order singular value decomposition to define weakly coupled and strongly correlated clusters: The n-body Tucker approximation," *Journal of Chemical Theory and Computation*, vol. 13, 2017.
[46] S. Chakraborty, Ö. T. Demir, E. Björnson, and P. Giselsson, "Efficient downlink power allocation algorithms for cell-free massive MIMO systems," *IEEE Open J. Commun. Society*, vol. 2, pp. 168–186, 2021.
[47] Y. Xiong, S. Sun, L. Qin, N. Wei, L. Liu, and Z. Zhang, "Performance analysis on cell-free massive MIMO with capacity-constrained fronthauls and variable-resolution ADCs," *IEEE Syst. J.*, pp. 1–12, 2021.
[48] H. Bolcskei, M. Borgmann, and A. J. Paulraj, "Impact of the propagation environment on the performance of space-frequency coded mimo-ofdm," *IEEE J. Sel. Areas Commun.*, vol. 21, no. 3, pp. 427–439, April 2003.
[49] 3GPP, "Further advancements for E-UTRA physical layer aspects (release 9)," 3GPP, Tech. Rep., March 2017.
[50] K. Haesek, *Design and Optimization for 5G Wireless Communications*.Wiley, 2020.
[51] P. C. Weeraddana, M. Codreanu, M. Latva-aho, A. Ephremides, and C. Fischione, "Weighted sum-rate maximization in wireless networks: A review," 2012.
[52] H. Iimori, G. T. F. de Abreu, and G. C. Alexandropoulos, "MIMO beamforming schemes for hybrid SIC FD radios with imperfect hardware and CSI," *IEEE Trans. Wireless Commun.*, vol. 18, no. 10, pp. 4816–4830, Oct. 2019.
[53] D. Tse and P. Viswanath, *Fundamentals of Wireless Communication*.Cambridge University Press, 2005.
[54] K. Shen, W. Yu, L. Zhao, and D. P. Palomar, "Optimization of MIMO device-to-device networks via matrix fractional programming: A minorization–maximization approach," *IEEE/ACM Trans. Networking*, vol. 27, no. 5, pp. 2164–2177, 2019.
[55] K. Shen and W. Yu, "Fractional programming for communication systems—part II: Uplink scheduling via matching," *IEEE Trans. Signal Process.*, vol. 66, no. 10, pp. 2631–2644, 2018.
[56] T. G. Kolda and B. W. Bader, "Tensor decompositions and applications," *SIAM Review*, 2008.
[57] P. H. Schoenemann, "A generalized solution of the orthogonal procrustes problem," *Psychometrika*, vol. 31, no. 1, 1966.
[58] H. Kenneth and K. Ray, *Linear Algebra. (2nd edition.)*.Cambridge University Press, 1972.
[59] Cheong Yui Wong, C. Y. Tsui, R. S. Cheng, and K. B. Letaief, "A real-time sub-carrier allocation scheme for multiple access downlink ofdm transmission," in *Proc. IEEE VTC-Fall*, vol. 2, 1999, pp. 1124–1128 vol.2.
[60] W. Rhee and J. M. Cioffi, "Increase in capacity of multiuser OFDM system using dynamic subchannel allocation," in *Proc. IEEE VTC-Spring, Tokyo, Japan*, vol. 2, 2000, pp. 1085–1089.
[61] F. Tan, P. Wu, Y.-C. Wu, and M. Xia, "Energy-efficient non-orthogonal multicast and unicast transmission of cell-free massive MIMO systems with SWIPT," *IEEE J. Sel. Areas Commun.*, vol. 39, no. 4, pp. 949–968, 2021.
[62] A.Ben-Tal and A.Nemirovski, *Lectures on Modern Convex Optimization: Analysis, Algorithms, and Engineering Applications*. SIAM, 2001.
[63] T. E. Bogale, L. B. Le, X. Wang, and L. Vandendorpe, "Pilot contamination mitigation for wideband massive mimo systems," *IEEE Transactions on Communications*, vol. 67, no. 11, pp. 7889–7906, 2019.

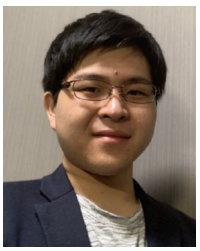

**KENGO ANDO** (Graduate Student Member, IEEE) received the B.E. and M.E. degrees in engineering from The University of Electro-Communications, Tokyo, Japan, in 2020 and 2022, respectively. He is currently pursuing the Ph.D. degree in electrical and computer engineering with Jacobs University Bremen, Germany. His current research interests are wireless communications and signal processing. He was a recipient of the YKK Graduate Fellowship for Master's students from the Yoshida Scholarship Foundation, Japan, from 2020 to 2022 and the Fellowship for overseas study in 2022 from the KDDI Foundation, Japan.

**HIROKI IIMORI** (Graduate Student Member, IEEE) received the B.Eng. and M.Eng. degrees (Hons.) in electrical and electronic engineering from Ritsumeikan University, Kyoto, Japan, in 2017 and 2019, respectively, and the Ph.D. degree (Hons.) in electrical engineering from Jacobs University Bremen, Bremen, Germany, in 2022. He was a Visiting Scholar with the Electrical the Computer Engineering Department, University of Toronto, Toronto, ON, Canada, in 2020. In 2021, he was a Research Intern with the Ericsson Radio S&R Research Laboratory, Yokohama, Japan. His research interests include optimization theory, wireless communications, and signal processing. He was awarded the YKK Doctoral Fellowship by Yoshida Scholarship Foundation, IEICE Young Researcher of the Year Award by the IEICE Smart Radio Committee in 2020, and IEICE RCS Active Research Award in 2018.

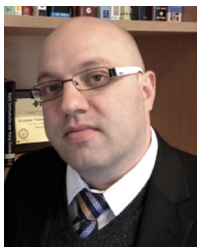

**GIUSEPPE THADEU FREITAS DE ABREU** (Senior Member, IEEE) received the B.Eng. degree in electrical engineering and the specialization (*Latu Sensu*) degree in telecommunications engineering from the Universidade Federal da Bahia (UFBa), Salvador, Bahia, Brazil, in 1996 and 1997, respectively, and the M. Eng. and D. Eng. degrees in physics, electrical and computer engineering from the Yokohama National University, Japan, in March 2001 and March 2004, respectively. He was a Postdoctoral Fellow and later an Adjunct Professor (Docent) on Statistical Signal Processing and Communications Theory with the Department of Electrical and Information Engineering, University of Oulu, Finland, from 2004 to 2006 and from 2006 to 2011, respectively. Since 2011, he has been a Professor of Electrical Engineering with Jacobs University Bremen, Germany. From April 2015 to August 2018, he also simultaneously held a full professorship with the Department of Computer and Electrical Engineering, Ritsumeikan University, Japan. His research interest spans a wide range of topics within communications and signal processing, including communications theory, estimation theory, statistical modeling, wireless localization, cognitive radio, wireless security, MIMO systems, ultra-wideband and millimeter wave communications, full-duplex and cognitive radio, compressive sensing, energy harvesting networks, random networks, connected vehicles networks, and many other topics. He was the co-recipient of best paper awards at several international conferences. He was also awarded the prestigious JSPS, Heiwa Nakajima, and NICT Fellowships in 2010, 2013, and 2015, respectively. He received the Uenohara Award by Tokyo University in 2000 for his Master's Thesis work. He served as an Associate Editor of IEEE TRANSACTIONS ON WIRELESS COMMUNICATIONS from 2009 to 2014, IEEE TRANSACTIONS ON COMMUNICATIONS from 2014 to 2017, and as an Executive Editor of IEEE TRANSACTIONS ON WIRELESS COMMUNICATIONS from 2017 to 2021.

**KOJI ISHIBASHI** (Senior Member, IEEE) received the B.E. and M.E. degrees in engineering from The University of Electro-Communications, Tokyo, Japan, in 2002 and 2004, respectively, and the Ph.D. degree in engineering from Yokohama National University, Yokohama, Japan, in 2007. From 2007 to 2012, he was an Assistant Professor with the Department of Electrical and Electronic Engineering, Shizuoka University, Hamamatsu, Japan. Since April 2012, he has been with the Advanced Wireless and Communication Research Center, The University of Electro-Communications, where he is currently a Professor. From 2010 to 2012, he was a Visiting Scholar with the School of Engineering and Applied Sciences, Harvard University, Cambridge, MA, USA. His current research interests are grant-free access, cell-free architecture, millimeter-wave communications, energy harvesting communications, wireless power transfer, channel codes, signal processing, and information theory.